ISSN: 2165-3259

JAOCR

Official Journal of the American Osteopathic College of Radiology

MUSCULOSKELETAL IMAGING

Guest Editor: Donald von Borstel, D.O.

Editor-in-Chief: William T. O'Brien, Sr., D.O.

July 2018, Vol. 7, Issue 3

JAOCR

Official Journal of the American Osteopathic College of Radiology

Aims and Scope

The Journal of the American Osteopathic College of Radiology (JAOCR) is designed to provide practical up-to-date reviews of critical topics in radiology for practicing radiologists and radiology trainees. Each quarterly issue covers a particular radiology subspecialty and is composed of high-quality review articles and case reports that highlight differential diagnoses and important teaching points.

Access to Articles

All articles published in the JAOCR are open access online. Subscriptions to the journal are not required to view or download articles. Reprints are not available.

Copyrights

Guide for Authors

Submissions for the JAOCR are by invitation only. If you were invited to submit an article and have questions regarding the content or format, please contact the appropriate Guest Editor for that particular issue. Although contributions are invited, they are subject to peer review and final acceptance.

Editor-in-Chief

Associate Editor

Editorial Board

JAOCR

MUSCULOSKELETAL RADIOLOGY

Guest Editor: Donald von Borstel, D.O.

From the Editor

Review Article

Differential-Based Case Reviews

JAOCR at the Viewbox

"All our dreams can come true, if we have the courage to pursue them."

Walt Disney

In this Issue

Donald von Borstel, D.O.

Adjunct Assistant Professor, Subspecialty Chief of the Musculoskeletal Division
Oklahoma State University Medical Center, Tulsa, OK

I would like to thank Dr. O'Brien and the JAOCR for giving me the chance to serve as guest editor for this musculoskeletal radiology issue. The process has given me the opportunity to highlight faculty members and residents I regularly work with at the Oklahoma State University Medical Center. I was also able to work with mentors and colleagues from the University of California, Irvine. Thank you to everyone who eagerly gave their time and dedicated work into completing this outstanding issue. A special thank you to my musculoskeletal mentor, Dr. Hiroshi Yoshioka, for his efforts in advancing MRI of the wrist through extensive research, as well as training the next generation of musculoskeletal radiologists.

The group of topics chosen for this issue was primarily meant to benefit the general practicing radiologist. We focused on topics within musculoskeletal radiology that a general radiologist would see on a normal day of practice. We chose to review extrinsic shoulder impingement and the associated MRI findings. This is a very common clinical entity that often leads to surgical intervention in symptomatic patients. Drs. Smith, Vassiliou, and Pack wrote an excellent review article concerning the important anatomy and pathology of the coracoacromial arch, which can contribute to rotator cuff impingement. The article will assist radiologists in understanding what MRI findings contribute to clinical symptoms of impingement and, in turn, allow them to create expert descriptions of these cases for referring surgeons.

Our other review article, MRI of the Wrist, serves as a companion resource for practicing radiologists when encountering wrist MRI cases. This article stems from my experience with MRI wrist imaging in fellowship, and I am honored to be writing this article with my mentor, Dr. Yoshioka, as well as Drs. Horiuchi and Strle. Reading wrist MRI can be a daunting task for many radiologists, and our aim is for this article to serve as a helpful guide.

The case review articles were chosen to highlight a wide range of musculoskeletal presentations. Drs. Lee and McCay review the differential diagnosis for an intermetatarsal lesion with the diagnosis of intermetatarsal bursitis. Also, Drs. Mason and Kirkland present a patient with a large lipomatous thigh mass. Our Viewbox articles were predominantly written by the radiology residents of Oklahoma State University Medical Center, who were instrumental in putting these articles together: Patellar Tendon-Lateral Femoral Condyle Friction Syndrome, Erosive Osteoarthritis, and Medial Tibial Stress Syndrome.

I am proud of this musculoskeletal radiology issue and thankful for all the authors and their essential contributions. My hope is that our issue entices radiology residents to pursue musculoskeletal radiology as a fellowship, which in my humble opinion, is the BEST specialty! In all seriousness, musculoskeletal radiology is an exciting field that takes continual education and lifelong study to serve as the sharp diagnostic tools that orthopedic specialists require. It is my pleasure to present the latest musculoskeletal issue for the JAOCR.

Last and most importantly, thank you to my wife for her love through the thick, and sometimes very thin, of the medical education process. I could not have gotten here without her unwavering support.

Shoulder Impingement and Associated MRI Findings

Cameron P. Smith, D.O., Christos E. Vassiliou, D.O., Jason R. Pack, M.D., Donald von Borstel, D.O.

Department of Radiology, Oklahoma State University Medical Center, Tulsa, OK

Shoulder pain is a common musculoskeletal medical condition affecting 7% to 26% of individuals and is the third most common musculoskeletal-related complaint in the primary care setting.[1,2] Rotator cuff pathology is a common etiology for shoulder pain, with impingement of the rotator cuff often playing an important role. Rotator cuff impingement was first described by Neer et al when he stated that 95% of rotator cuff tears were attributed to impingement and generally occur in patients over age 40.[3,4] Two predominant types of shoulder impingement have been described: intrinsic and extrinsic.

Intrinsic shoulder impingement is relatively uncommon and seen almost exclusively with overhead throwing athletes.[5] It is a result of extreme abduction and external rotation, which can lead to entrapment of the supraspinatus and/or the infraspinatus tendons between the glenoid.[6] MRI appearance of intrinsic impingement is varied and includes labral and rotator cuff pathology. The infraspinatus tendon is commonly injured, especially in patients under age 30, with MRI findings ranging from undersurface tears to complete tears.[6,7]

Extrinsic, or external, impingement is one of the more common causes of shoulder pain and a frequent source for an orthopedic evaluation.[8] Extrinsic shoulder impingement is most commonly related to mechanical compression from the acromion, acromioclavicular joint, and the coracoacromial ligament.[3,9] Numerous operative and nonoperative treatment options have been described for extrinsic impingement, ranging from physical therapy and injections to acromioplasty and Mumford procedures.

The purpose of this article is to help understand the relevant anatomy with regard to the subacromial region, review the imaging findings, and discuss the differing etiologies of extrinsic impingement. This knowledge will allow radiologists to effectively communicate with clinicians and help guide appropriate treatment.

Anatomy

The coracoacromial arch provides a safeguard for the shoulder, limiting superior migration of the humeral head. The coracoacromial arch is composed of (from anterior to posterior) the coracoid process, coracoacromial ligament, and the acromion process. Inferior to these structures, and coursing through the arch, are the subacromial/subdeltoid bursa, supraspinatus tendon, and biceps tendon. The humeral head provides the posterior/inferior border of the arch **(Figure 1).** Processes that decrease the space within the coracoacromial arch presumably may lead to impingement-like symptoms.

The *coracoid process* is a hook-like osseous structure arising from the superolateral edge of the scapula and extends in an anterolateral orientation. The coracoid is an anchor point for several ligaments and tendons, including the pectoralis minor, coracobrachialis, and short head of the biceps brachii tendons. Also, the coracoid is an attachment site for the coracohumeral, coracoacromial, coracoclavicular, and superior transverse ligaments.[10] The coracoid process can be palpated below and at the lateral edge of the clavicle. Known as the "Surgeon's Lighthouse," the coracoid process serves as a landmark to avoid neurovascular injury, as major neurovascular structures traverse medially to the coracoid process.[11]

The *coracoacromial ligament* is a thick triangular ligamentous structure extending inferomedially from the anterolateral undersurface of the acromion to the lateral border of the coracoid process. This structure provides an

FIGURE 1. *Subacromial space. PD sagittal image demonstrating the subacromial space including the coracoid (asterisk), coracohumeral ligament (dashed arrow), and supraspinatus muscle/tendon (solid arrow).*

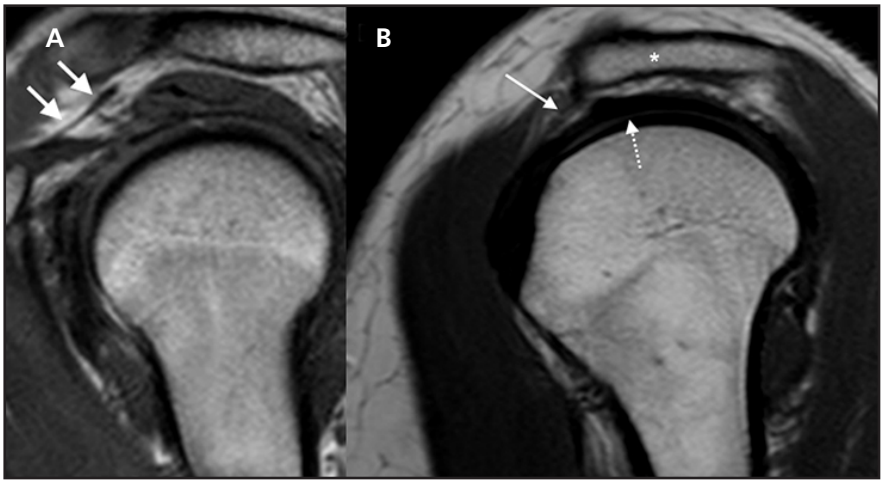

FIGURE 2. *Subacromial space and coracoacromial ligament. Sagittal PD (A) and T1WI (B) showing the relationship of the subacromial space, coracoacromial ligament (solid arrow), supraspinatus tendon (dashed arrow), and acromion (asterisk).*

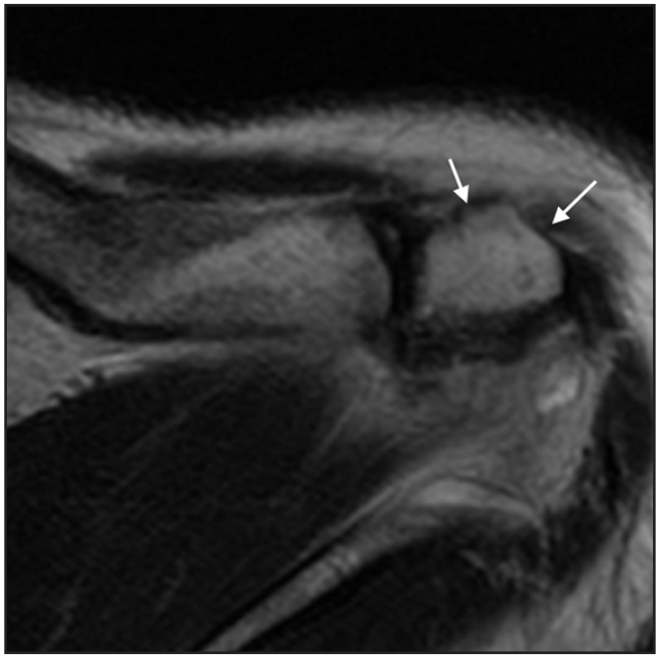

FIGURE 3. *Unfused ossification center. Axial PD sequence showing a corticated osseous structure (solid arrows) articulating with the clavicle, representing an unfused secondary ossification center. This is consistent with a meso-type os acromiale without marrow edema or degenerative changes.*

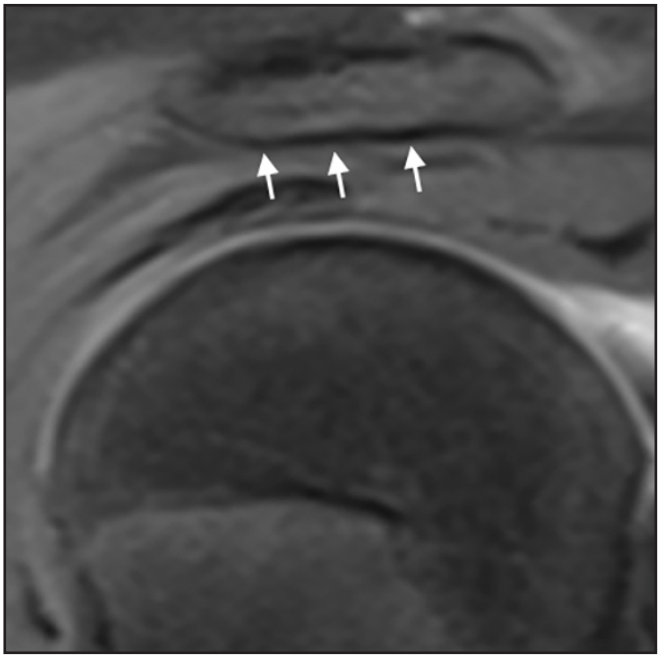

FIGURE 4. *Type I acromion. Sagittal T1-weighted fat-suppressed sequence after intraarticular injection of contrast displays flattening of the undersurface of the lateral acromion (solid arrows), which is consistent with a Bigliani type I acromion.*

osseo-ligamentous static restraint to superior humeral head displacement. Ligamentous connection of the coracoacromial ligament and the rotator interval capsule is thought to prevent inferior migration of the glenohumeral joint.[12] Coracoacromial ligament thickness is normally 2 to 5.6 mm.[13] Implicated as a pain generator in impingement syndrome, treatment of the coracoacromial ligament has been controversial. There is uncertainty regarding whether or not to perform a release of the coracoacromial ligament during acromioplasty, as this could increase the risk of superior and anterior glenohumeral translation.[9]

The *acromion process* is a triangular-like extension of the scapular spine, and anteriorly articulates with the clavicle. The acromioclavicular articulation is a synovial joint, connecting the scapula and clavicle, allowing the scapula to have multidirectional motion with relation to the rest of the body. The coracoacromial ligament forms the ligamentous attachment between the acromion and coracoid process **(Figure 2)**. The deltoid and trapezius muscle groups have attachments on the acromion. The

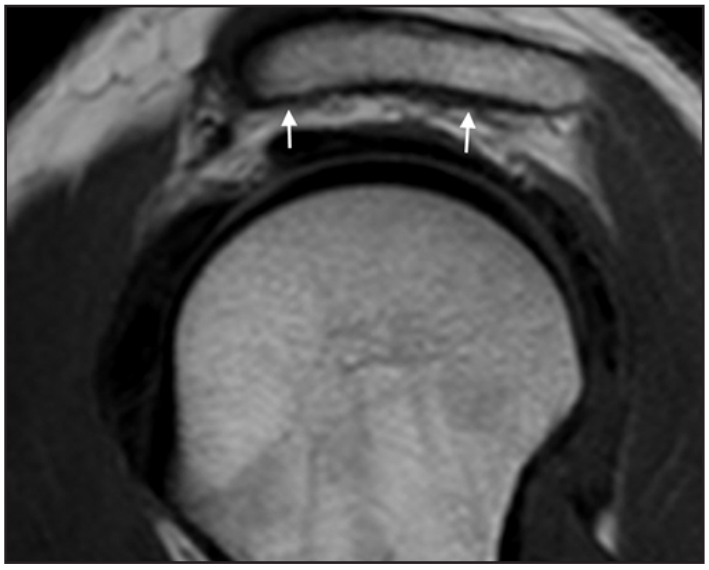

FIGURE 5. *Type II acromion. Sagittal T1WI demonstrating a concave undersurface (solid arrows) of the lateral acromion consistent with a Bigliani type II acromion.*

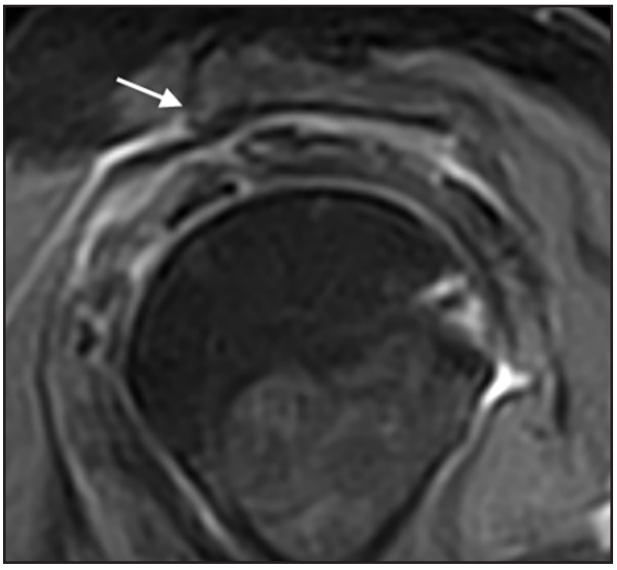

FIGURE 6. *Type III acromion. Sagittal T2-weighted fat-suppressed image demonstrating an anterior-inferior hook of the lateral acromion (solid arrow) consistent with a Bigliani type III acromion.*

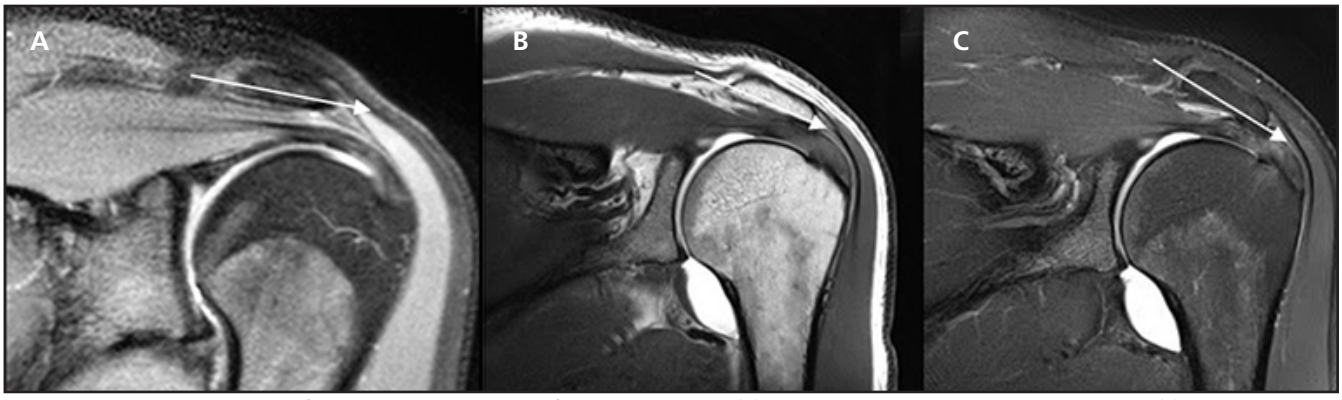

FIGURE 7. *Lateral downsloping of the acromion. Coronal PD fat-saturated image (A) with a normal acromial slope. T1-weighted (B) and T2-weighted fat-suppressed (C) images demonstrating lateral downsloping of the acromion (solid arrows).*

FIGURE 8*. Low-lying acromion. Coronal T1-weighted image with intra-articular contrast displaying a low-lying acromion (solid arrow) in relation to the clavicle (open arrow) with the inferior acromion cortex below the inferior cortex of the clavicle.*

deltoid muscle abducts the arm at the shoulder and contraction of the trapezius rotates the scapula, providing stability to the scapular body. At birth, the distal acromion and clavicle are cartilaginous structures, but maintain the shape of the fully matured ossified bone. With maturation, the primary ossification center ossifies and proceeds to fuse with smaller secondary ossification centers to form a single fused plate. Most literature suggests these ossification centers normally ossify between 18 to 25 years of age.[14] Unfused secondary ossification centers may be mistaken for avulsion fractures, and primary and secondary fusion scars can mimic an incompletely healed fracture on radiographs and MRI, respectively **(Figure 3)**. The presence of marrow edema on MR images should portend a diagnosis of fracture.[15]

As stated earlier, Neer proposed that tears of the cuff tendons (specifically the supraspinatus) are often a result of impingement by structures forming the coracoacromial arch. Extrinsic impingement syndrome is clinically characterized as acute or chronic pain induced by abduction and external rotation or elevation with internal rotation of the shoulder. Impingement typically occurs in young athletes who participate in sports involving repetitive movements of elevation and abduction of the shoulder, or in the elderly population with degenerative joint disease.[16] Numerous anatomical etiologies have

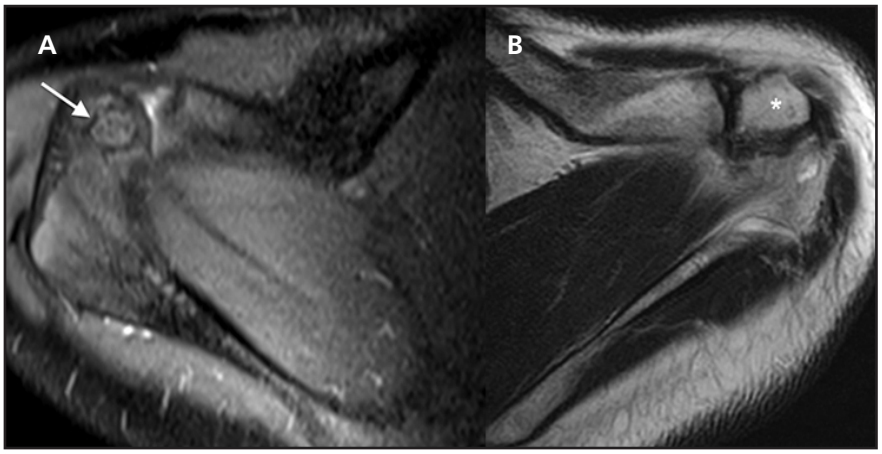

FIGURE 9. *Os acromiale. Axial T2-weighted fat-suppressed image (A) showing a pre-acromion os acromiale (solid arrow) with mild reactive marrow edema-like signal. Axial T2-weighted image (B) showing a meso-acromion os acromiale (asterisk).*

FIGURE 10. *Subacromial/subdeltoid bursitis. Coronal short tau inversion recovery (STIR) image with subacromial/subdeltoid bursitis. STIR hyperintense fluid-like signal distends the bursal sac > 3 mm in thickness. Also, the fluid extends 2 cm medial to the acromioclavicular joint (solid arrows).*

been suggested as a contributor of impingement syndrome including variant acromion shape, slope of the acromion, acromioclavicular arthropathy, acromion positioning, coracoacromial ligament thickening, and os acromiale. However, it is worth noting that many of the aforementioned anatomical factors can be seen in the asymptomatic patient, and ultimately the diagnosis is one of a clinical nature.[17]

Three predominant shapes of the lateral acromion have been described by Bigliani et al and are based on the scapular-Y view radiograph.[18] Type I acromion has a flat undersurface **(Figure 4)**. Type II acromion is more concave along the undersurface with the inferior acromial cortex parallel to the cortex of the humeral head **(Figure 5)**. Type III acromion has an inferiorly projecting anterior hook, narrowing the space between the acromion and humeral head **(Figure 6)**. Some theories suggest type II and III acromions have an increased incidence of cuff disease, but this remains controversial among most surgeons.[17] Type IV acromion has also recently been described as having a convex undersurface, although correlation with extrinsic impingement has not been shown.[19,20]

Normal orientation of the lateral aspect of the acromion is horizontal or slightly downsloping posteriorly on the sagittal images. An abnormally sloped acromion occurs in an anteriorly downsloped and inferolateral sloped orientation **(Figure 7)**. These anomalous acromial sloping positions can impinge on the subacromial space and cause mechanical trauma to the subjacent supraspinatus tendon.[17]

Normal positioning of the acromion has an inferior cortex running parallel with the inferior cortex of the clavicle. When the acromion is low-lying, the inferior cortex of the acromion lies below the inferior cortex of the clavicle **(Figure 8)**. This low position causes narrowing of the subacromial space.[17]

Os acromiale represents an accessory ossification center that has not fused by age 25 years. This normal variant occurs in 15% of the population. Failure of fusion occurs between 1 of the 3 ossification centers: pre-acromion **(Figure 9A)**, meso-acromion **(Figure 9B)**, and meta-acromion. A classification scheme was proposed by Park et al with subtypes A-G**.** Type A, also known as the meso-acromial or meso-type, is the most common and is a failure of fusion between the meso-acromion and meta-acromion.[21] The presence of an os acromiale has been associated with increased incidence of impingement and rotator cuff disease,

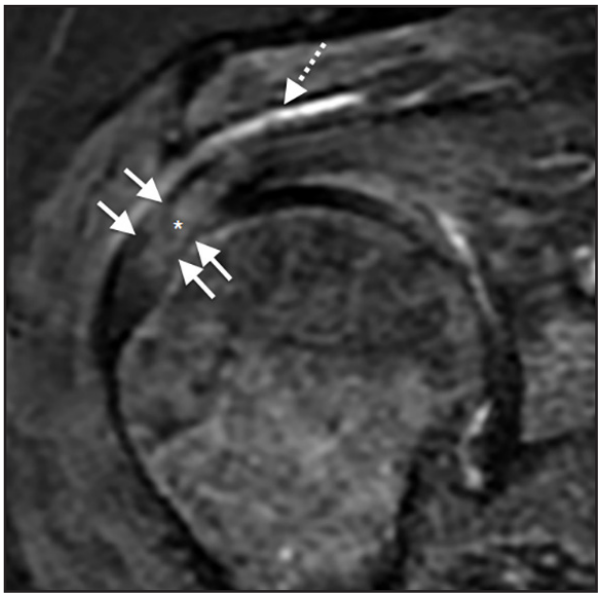

FIGURE 11. *Coronal STIR image showing supraspinatus tendinosis/tendinopathy. There is intermediate intrasubstance signal intensity (asterisk) within the thickened supraspinatus tendon. This signal is hypointense compared to intra-articular fluid signal. The bursal and articular surface fibers are intact (solid arrows). There is also incidentally mild subacromial/subdeltoid bursitis with fluid-like signal in the bursa (dashed arrow).*

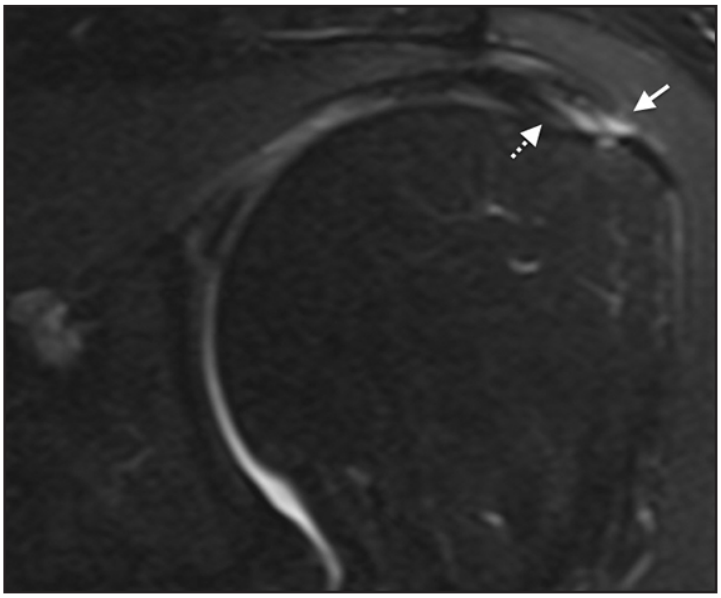

FIGURE 12. *Bursal surface partial thickness rotator cuff tear. Coronal T2-weighted fat-suppressed image with bursal surface hyperintense signal involving > 50% of the supraspinatus tendon footprint depth (solid arrow) with intact articular surface fibers (dashed arrow). This is consistent with a grade III partial bursal surface supraspinatus tear.*

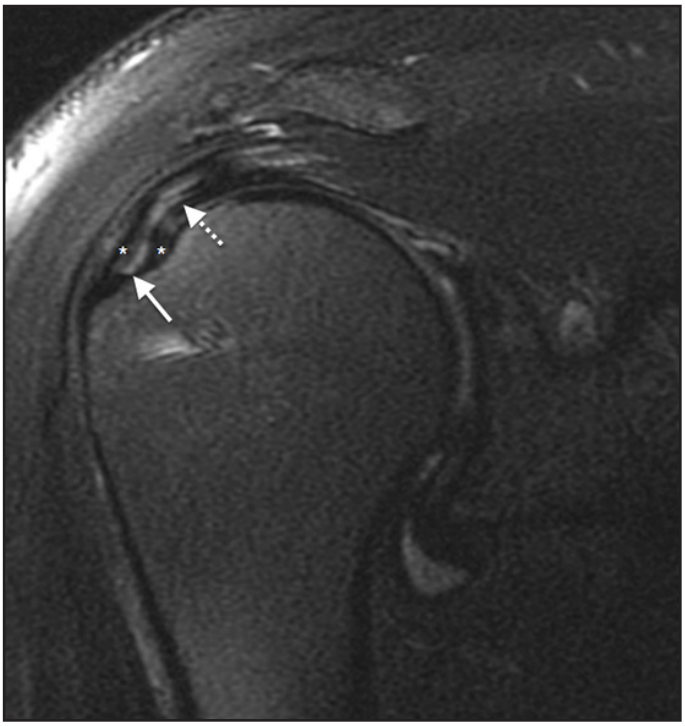

FIGURE 13. *Intrasubstance partial thickness rotator cuff tear. Coronal PD fat-suppressed image showing an intrasubstance tear of the supraspinatus tendon at the footprint (solid arrow) measuring < 3mm, consistent with a grade I partial tear. Linear longitudinal signal propagates from the footprint into the substance of the tendon (dashed arrow), which represents an interstitial/delaminating component. Intact bursal and articular surface fibers are at the tendon footprint (asterisk).*

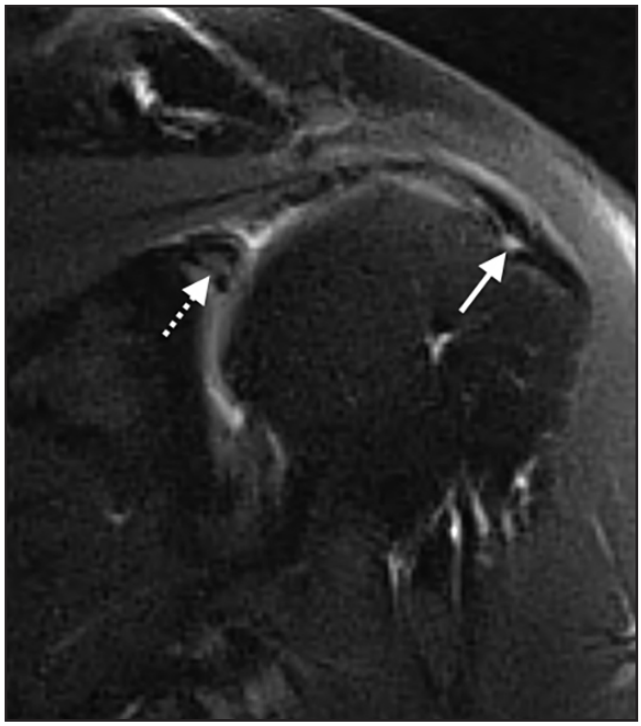

FIGURE 14. *Articular surface partial thickness rotator cuff tear. Coronal T2-weighted fat-suppressed image showing focal articular surface hyperintense signal (solid arrow) involving < 50% of the tendon depth. An incidental superior labral tear is also seen (dashed arrow).*

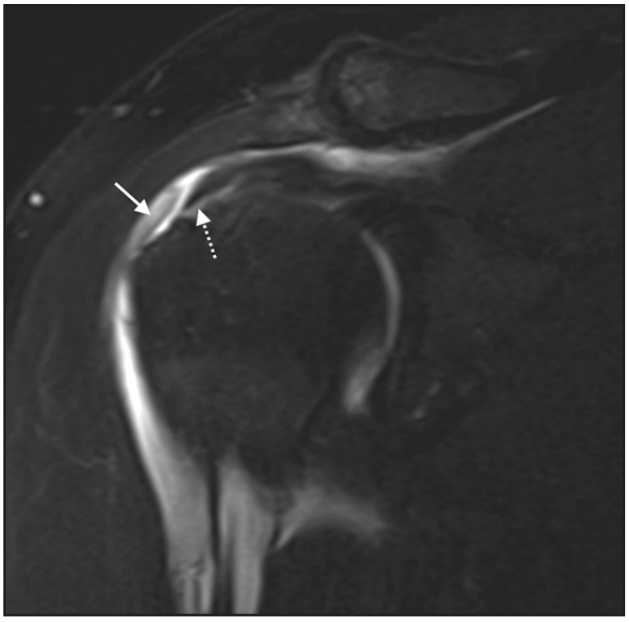

FIGURE 15. *Full thickness rotator cuff tear. Coronal T2-weighted fat-suppressed image with intra-articular contrast displaying a full-thickness defect extending through the bursal and articular surfaces of the supraspinatus tendon (solid arrow). There is minimal retraction of the tendon from the footprint (dashed arrow). Contrast is extending through the tear into the subacromial/subdeltoid space.*

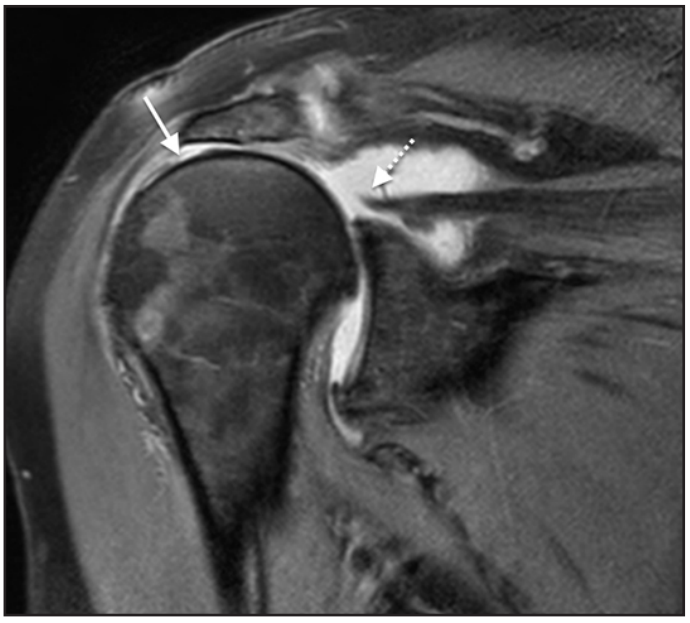

FIGURE 16. *Full thickness rotator cuff tear with retraction. Coronal PD fat-suppressed image showing a full-thickness tear (solid arrow) of the supraspinatus tendon. Retraction of the tendon is > 5 cm from the footprint, medial to the glenoid (dashed arrow). Retraction medial to the glenoid is an indication of a tear not usually amenable to repair. Incidentally, there is cephalization of the humeral head nearly abutting the undersurface of the acromion secondary to complete rotator cuff tear*

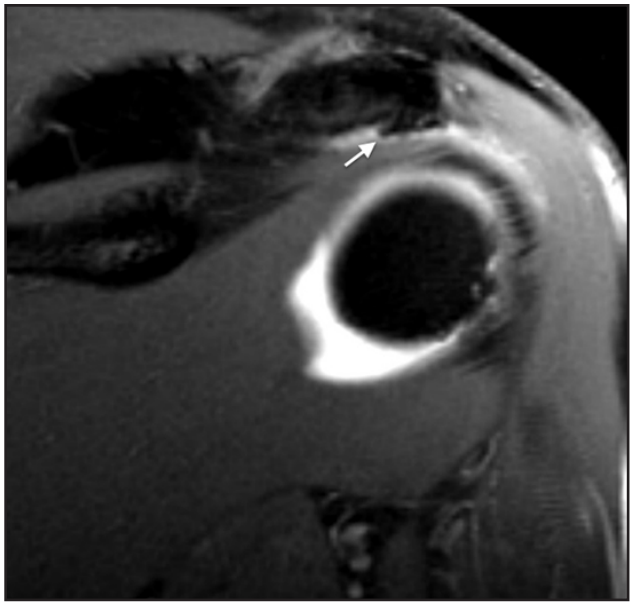

FIGURE 17. *Subacromial spurs. Coronal PD fat-suppressed image showing a keel osteophyte (solid arrow) along the anterolateral undersurface of the acromion. The keel osteophyte is an aggressive spur often resulting in severe damage to the bursal cuff.*

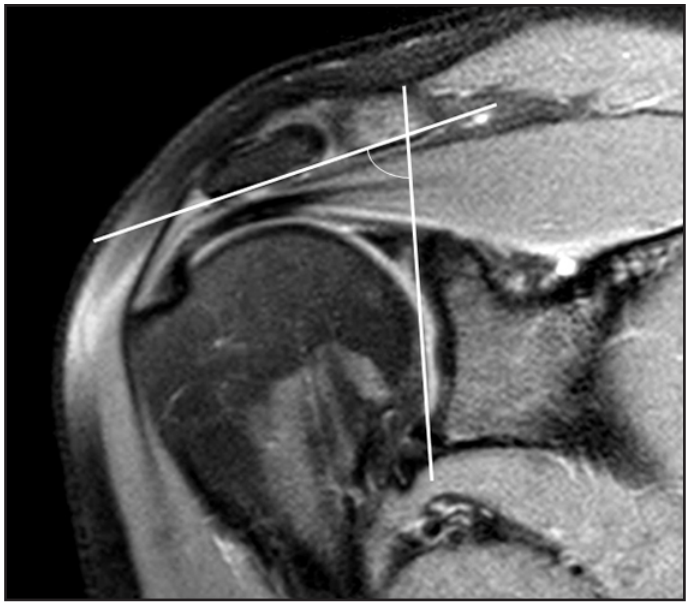

FIGURE 18*. Lateral acromial angle. Coronal PD fat-suppressed image with a normal lateral acromion angle. This angle is formed by a vertical line lateral to the glenoid and a line parallel to the undersurface of the acromion. Normal angle is > 70 degrees.*

although is controversial in the literature.[21,22] There is suggestion that the os is mobile, and thus reduces the size of the coracoacromial arch during motion. Os acromiale can cause impingement in 2 separate manners: Contraction of the deltoid muscle will force the os acromiale inferiorly, leading to narrowing of the rotator cuff outlet. The other mechanism occurs when osteophytes develop at the margin of the acromial gap, often directly impinging on the rotator cuff.

Imaging Appearance of Extrinsic Impingement

The imaging findings of external impingement are varied, ranging from subacromial/subdeltoid bursitis to full-thickness rotator cuff tears. In

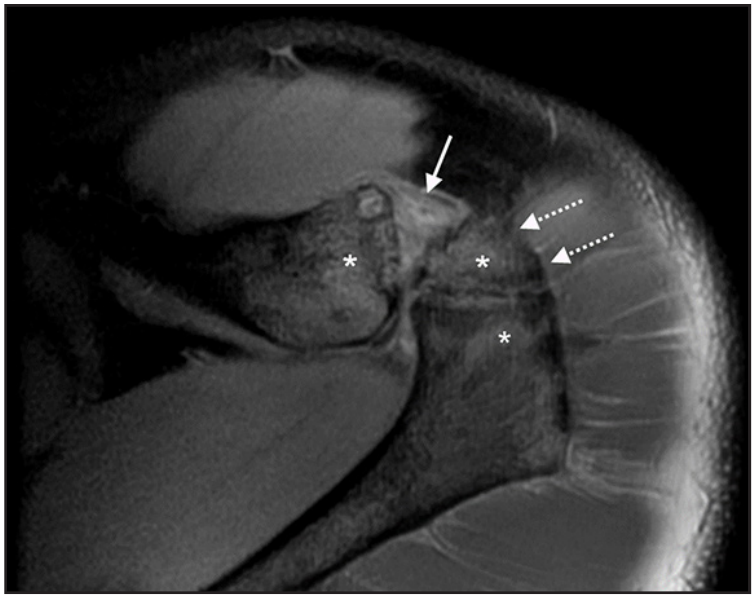

FIGURE 19. *Unstable os acromiale. Axial fat-suppressed PD image with a meso-type os acromiale (dashed arrows). There is acromioclavicular joint space edema (solid arrow) with reactive marrow edema of the acromion, os acromiale, and distal clavicle (asterisks). This is consistent with an unstable os acromiale.*

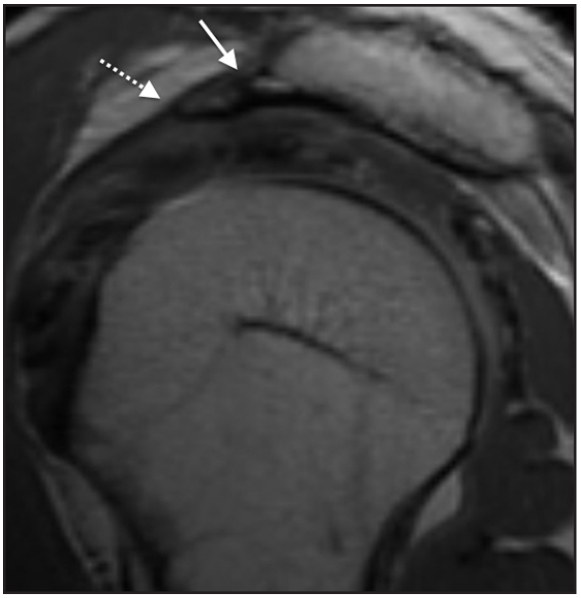

FIGURE 20. *Coracoacromial ligament thickening. Sagittal T1-weighted image with thickening of the coracoacromial ligament measuring > 6 mm (dashed arrow), and a spur at the acromion attachment (solid arrow).*

1972, Charles Neer classified impingement into 3 distinct stages. Stage I impingement is characterized by edema and/or hemorrhage in the subacromial/subdeltoid bursa and is generally seen in patients less than 25 years-old. Stage II demonstrates chronic changes such as fibrosis and tendinitis of the rotator cuff and is generally seen in those 25 to 40 years. Stage III is characterized by partial or complete rotator cuff tears, and is usually seen in patients > 40 years.[4,23]

Subacromial/subdeltoid bursitis is a finding seen with considerable frequency on MRI examinations of the shoulder **(Figure 10)**. This diagnosis is characterized by fluid-like signal in the bursa that extends 2 cm medial to the acromioclavicular joint with distension of the bursa > than 3 mm thick. Fluid also commonly extends into the anterior aspect of the bursa.[24]

Rotator cuff tendinopathy (or tendinosis) is depicted by thickening and increased signal within the tendons. With tendinopathy, there is no visible discontinuity of tendon fibers and signal does not extend to the articular or bursal surface. Also, signal seen within tendinopathy is hyperintense on fluid-sensitive sequences, but is hypointense compared to nearby intra-articular fluid signal **(Figure 11)**. Fluid-like hyperintense signal within the tendon suggests an intrasubstance partial tear.

Partial thickness tears of the rotator cuff are characterized by fluid-like signal in the tendons that does not involve the entire tendon bulk. These tears can be further characterized by whether they involve the bursal surface, intrasubstance portion of the tendon, or articular surface of the tendon fibers **(Figures 12-14)**. Partial thickness tears occur more frequently along the articular surface of the tendon.[25] Ellman developed a classification system for partial rotator cuff tears based on the tendon tear depth. This system classifies partial thickness tears into grade I (< 3 mm), grade II (3 to 6 mm), or grade III (> 6 mm).[26] As grade III tears comprise > 50% of the rotator cuff, these are generally considered significant and are typically repaired surgically.[27]

Full-thickness rotator cuff tears are manifested by fluid-like signal within the tendon, which extends throughout the entire substance of the tendon from the articular to the bursal surface **(Figure 15)**. These can be further classified according to size. A widely used system created by DeOrio and Cofield classifies full thickness tears based on their greatest dimension. These are classified as small (< 1 cm), medium (1 to 3 cm), large (3 to 5 cm), or massive (> 5 cm).[28] Other important features of full-thickness tears are the degree of tendon retraction and presence or absence of muscle atrophy. A tendon retracted medial to the glenoid has historically indicated that the tendon tear is not amenable to repair **(Figure 16)**.[29] Muscle atrophy in association with a full-thickness tear of the supraspinatus or infraspinatus tendons suggests that the muscle has lost its ability to contract and may not be successfully treated with surgery.[30] This information is of clinical value to the surgeon when deciding whether to repair the tear.

MR characteristics of impingement have been subsequently grouped into subtypes by Seeger et al.[31] Type I impingement is noted as the least severe and includes subacromial bursitis and bursal thickening with normal signal intensity of the supraspinatus tendon. Type II impingement is classified as abnormally high-signal in the supraspinatus tendon without abnormal intramuscular signal or tendon retraction.

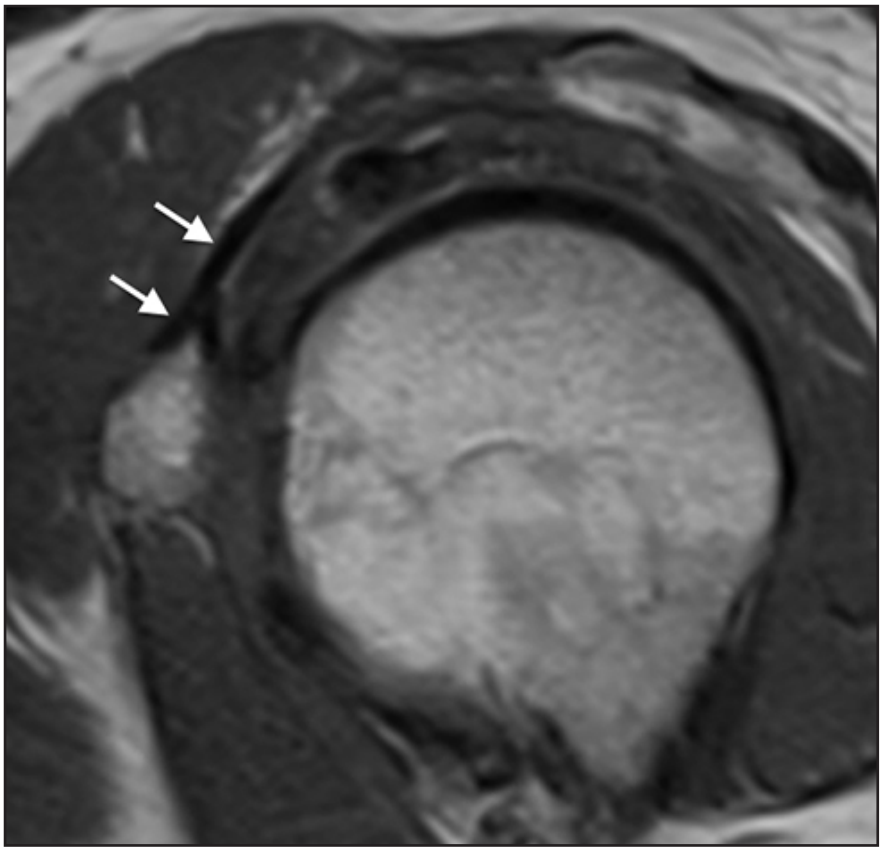

FIGURE 21. *Coracoacromial ligament thickening. Sagittal T1-weighted image with thickening of the coracoacromial ligament at the coracoid attachment (solid arrows) measuring > 6 mm.*

Type III impingement findings include full-thickness abnormal signal intensity with muscle retraction, indicating a full-thickness tear.

Acromion morphology and acromion-related pathology is easily identified on MR. Acromial spurs have been described with numerous morphologic subtypes including acromial hook and keel osteophytes. The acromial hook lies within the origin of the coracoacromial ligament and projects toward the coracoid. This is located at the anterior inferior acromion.[32] A subacromial keel osteophyte is an acromial spur that causes severe damage to the bursal cuff and is shaped like the keel of a sailboat. The spur is found along the anterior lateral edge of the acromion, between the lateral border of the acromion and the acromioclavicular joint, and extends posteriorly to the middle of the acromion undersurface.[33]

Location of the acromial spur is also important, occurring along the medial, lateral, and anterior aspects of the acromion with anterolateral spurs having a closer association with cuff pathology.[34]

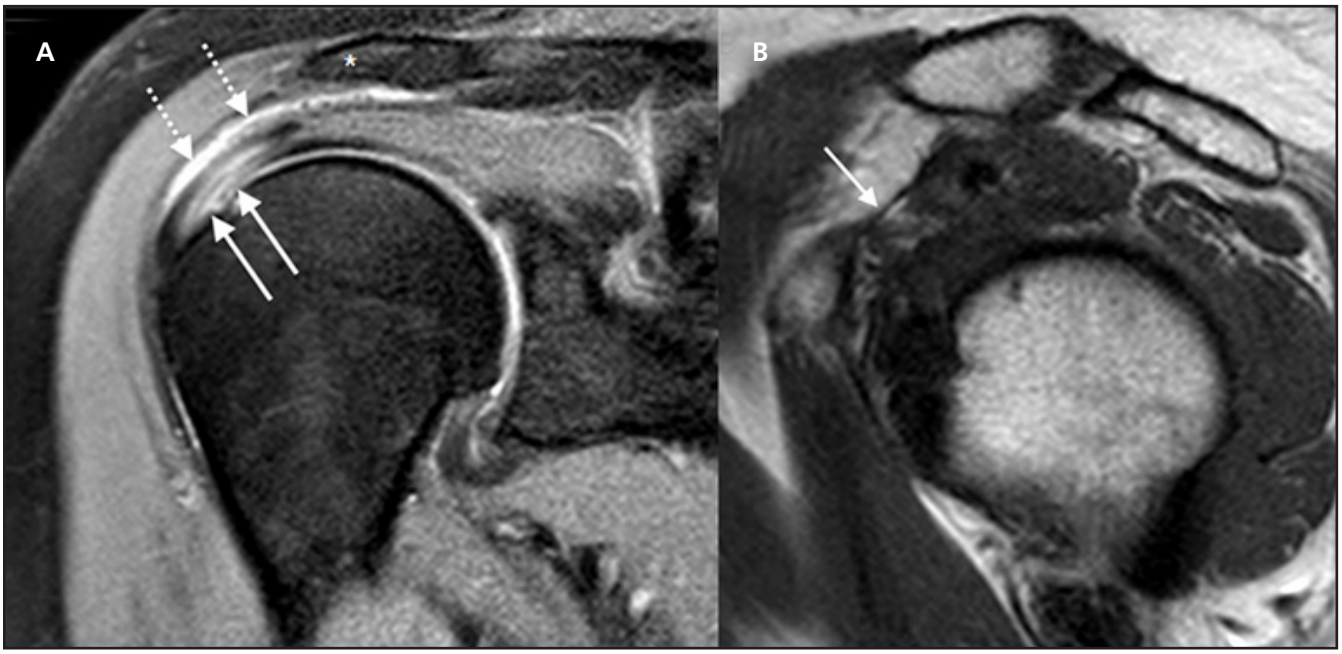

FIGURE 22. *Subacromial decompression. Coronal PD fat-saturated image (A) showing flattening of the undersurface of the acromion (asterisk) consistent with acromioplasty. Also visualized is partial thickness articular surface intermediate signal (solid arrows) consistent with chronic partial tear of the supraspinatus tendon. Hyperintense bursal signal (dashed arrows) is consistent with mild subacromial/subdeltoid bursitis. Sagittal T1-weighted image (B) of the same patient showing thinning of the coracoacromial ligament near the coracoid attachment (solid arrow), which is consistent with a prior ligamentous release.*

Subacromial spurs are contiguous with the cortex of the acromion undersurface with signal isointense to adjacent bone marrow on MRI **(Figure 17)**. Acromion shape has been implicated in impingement with a classification scheme devised by Bigliani et al, as described previously. Only type III has shown a common association with impingement and rotator cuff tears, by most authors. Impingement and rotator cuff tears attributed to a type III acromion are best appreciated on the coronal and sagittal sequences.[20,35] The slope and angle of the acromion is also associated with extrinsic impingement. Studies have indicated that low lateral acromial angle was seen with a higher incidence of impingement. Lateral acromial angle is calculated by a vertical line lateral to the glenoid and a horizontal line parallel to the acromion surface **(Figure 18)**. Lateral acromial angle can be seen effectively on the coronal MR image with an angle < 70 degrees associated with cuff pathology.[20,36]

Evaluating an os acromiale and its contribution to impingement can be challenging. On coronal and sagittal planar imaging, an os acromiale may be mistaken for a normal acromioclavicular joint. Axial imaging, usually the most cephalad image, is ideal for identifying an os acromiale. High-signal intensity on T2-weighted images may be appreciated at the synchondrosis, which may represent degenerative changes and/or instability of the os acromiale **(Figure 19)**.[21,37]

Acromioclavicular joint osteoarthritis may result in inferior projecting osteophytes or fibrosis around the joint capsule, potentially causing impingement. Inferior spurring of the distal clavicle and acromion can also cause impingement, with an inferior acromial spur associated more often with clinical symptoms. MRI appearance varies and acromioclavicular arthrosis may demonstrate marrow edema (which will have high signal intensity on T2-weighted sequences), subchondral cysts, sclerosis, and/or erosions.[38]

Coracoacromial ligament (CAL) pathology has been extensively studied with regard to impingement syndrome.[39] The CAL is susceptible to pathological degeneration, which can thicken the ligament, greater than its normal thickness of 2 to 5.6 mm. This thickening, and associated subacromial osteophytes at the ligamentous attachment, can cause impingement on the supraspinatus tendon **(Figures 20, 21)**.[40]

Treatment

Of the nonoperative treatment options, studies have shown that exercise therapy combined with other noninvasive treatments have higher efficacy with regard to pain score.[41] Exercise therapy and localized drug injections showed better positive effects on pain score than any other nonoperative treatment options.[41,42]

Operative treatment options for extrinsic shoulder impingement are usually related to the underlying etiological cause, and are usually reserved for cases of failed conservative treatments. One of the more common surgical procedures is subacromial decompression, which involves a subacromial bursectomy, release or retraction of the coracoacromial ligament, and removal of the subacromial spurs **(Figure 22)**. This can be performed either as open surgery or arthroscopically. Some studies have shown that an arthroscopic approach has a better efficacy, while others show no significant difference in long-term outcome. However, it is generally accepted that arthroscopy has less of an economic burden and should be the preferred method.[43,44]

CAL release is a controversial topic and resection can lead to biomechanical alteration with regard to humeral head movement. Therefore, partial release has been advocated with good long-term outcomes.[39,45] Limited studies have evaluated bursectomy alone vs. standard subacromial decompression, with no significant difference in clinical results between the procedures.[46] Acromioclavicular joint arthritis alone can be a source of pain, but has also been implicated as a cause of impingement. Distal clavicular resection, or the Mumford procedure, has been shown to improve symptomatic impingement with related acromioclavicular arthropathy as an adjunct to subacromial decompression.[47,48] Os acromiale treatment includes conservative measures, although patients with persistent symptomatic or functional deficits can benefit from surgical options. One of the more common procedures is an osseous fusion of the os acromiale combined with internal fixation and tension banding. This is usually followed by acromioplasty of the new acromio-acromion joint, ie, a 2-stage fusion.[49]

Conclusion

Extrinsic shoulder impingement is a common cause of shoulder pain and frequently seen in clinical practice. Imaging plays an important role in identifying the cause of impingement and also in guiding clinicians with treatment planning. Understanding the anatomy, underlying mechanics, and MRI characteristics of rotator cuff impingement will allow for prompt recognition and ultimately improve outcomes.

References

1. Luime JJ, Koes BW, Hendriksen IJM, et al. Prevalence and incidence of shoulder pain in the general population; a systematic review. Scand J Rheumatol 2004;33(2):73-81.
2. Urwin M, Symmons D, Allison T, et al. Estimating the burden of musculoskeletal disorders in the community: the comparative prevalence of symptoms at different anatomical sites, and the relation to social deprivation. Ann Rheum Dis 1998;57(11):649-655.
3. Neer CS. Impingement lesions. Clin Orthop Relat Res 1983;173:70.
4. Wolff AB, Sethi P, Sutton KM, et al. Partial thickness rotator cuff tears. J Am Acad Orthop Surg 2006;14(13):715.
5. Budoff JE, Nirschl RP, Ilahi OA, et al. Internal impingement in the etiology of rotator cuff tendinosis revisited. Arthroscopy 2003;19(8):810-814.
6. Giaroli EL, Major NM, Higgins LD. MRI of internal impingement of the shoulder. Am J Roentgenol 2005;185(4):925-929.
7. Muto T, Inui H, Ninomiya H, et al. Characteristics and clinical outcomes in overhead sports athletes after rotator cuff repair. J Sports Med 2017;2017:5476293.
8. Seitz AL, McClure PW, Finucane S, et al. Mechanisms of rotator cuff tendinopathy: intrinsic, extrinsic, or both? Clin Biomech 2011;26(1):1-12.
9. Neer CS 2nd. Anterior acromioplasty for the chronic impingement syndrome in the shoulder: a preliminary report. J Bone Joint Surg Am 1972;54(1):41-50.

10. Standring S. Gray's Anatomy E-Book: The Anatomical Basis of Clinical Practice. Amsterdam, Netherlands: Elsevier Health Sciences; 2015.
11. Matsen FA. Shoulder Surgery: Principles and Procedures. Philadelphia, PA: Saunders; 2004.
12. Edelson JG, Luchs J. Aspects of coracoacromial ligament anatomy of interest to the arthroscopic surgeon. Arthroscopy 1995;11(6):715-719.
13. Gallino M, Battiston B, Annaratone G, et al. Coracoacromial ligament: a comparative arthroscopic and anatomic study. Arthroscopy 1995;11(5):564-567.
14. Scheuer L, Black S, Christie A. The pectoral girdle. San Diego, CA: Elsevier Academic Press; 2000.
15. Flecker H. Roentgenographic observations of the times of appearance of epiphyses and their fusion with the diaphyses. J Anat 1932;67(Pt 1):118-164.3.
16. Rockwood CA, Lyons FR. Shoulder impingement syndrome: diagnosis, radiographic evaluation, and treatment with a modified Neer acromioplasty. J Bone Joint Surg Am 1993;75(3):409-424.
17. Michener LA, McClure PW, Karduna AR. Anatomical and biomechanical mechanisms of subacromial impingement syndrome. Clin Biomech 2003;18(5):369-379.
18. Bigliani LU, D'Alessandro DF, Duralde XA, et al. Anterior acromioplasty for subacromial impingement in patients younger than 40 years of age. Clin Orthop Relat Res 1989;(246):111-116.
19. Farley TE, Neumann CH, Steinbach LS, et al. The coracoacromial arch: MR evaluation and correlation with rotator cuff pathology. Skeletal Radiol 1994;23(8):641-645.
20. Balke M, Schmidt C, Dedy N, et al. Correlation of acromial morphology with impingement syndrome and rotator cuff tears. Acta Orthop 2013;84(2):178-183.
21. Park JG, Lee JK, Phelps CT. Os acromiale associated with rotator cuff impingement: MR imaging of the shoulder. Radiology 1994;193(1):255-257.
22. Rovesta C, Marongiu MC, Corradini A, et al. Os acromiale: frequency and a review of 726 shoulder MRI. Musculoskelet Surg February 2017. doi:10.1007/s12306-017-0463-2.
23. De Yang Tien J, Tan AHC. Shoulder impingement syndrome, a common affliction of the shoulder: a comprehensive review. Proc Singapore Healthcare 2014;23(4):297-305.
24. Umer M, Qadir I, Azam M. Subacromial impingement syndrome. Orthop Rev 2012;4(2):e18.
25. Vinson EN, Helms CA, Higgins LD. Rim-rent tear of the rotator cuff: a common and easily overlooked partial tear. Am J Roentgenol 2007;189(4):943-946.
26. Ellman H. Diagnosis and treatment of incomplete rotator cuff tears. Clin Orthop Relat Res 1990;254:64.
27. Weber SC. Arthroscopic debridement and acromioplasty versus mini-open repair in the treatment of significant partial thickness rotator cuff tears. Arthroscopy 1999;15(2):126-131.
28. DeOrio JK, Cofield RH. Results of a second attempt at surgical repair of a failed initial rotator-cuff repair. J Bone Joint Surg Am 1984;66(4):563-567.
29. Thomazeau H, Boukobza E, Morcet N, et al. Prediction of rotator cuff repair results by magnetic resonance imaging. Clin Orthop Relat Res 1997;(344):275-283.
30. Maughan RJ, Watson JS, Weir J. Strength and cross-sectional area of human skeletal muscle. J Physiol 1983;338:37-49.
31. Seeger LL, Gold RH, Bassett LW, et al. Shoulder impingement syndrome: MR findings in 53 shoulders. Am J Roentgenol 1988;150(2):343-347.
32. Ogata S, Uhthoff HK. Acromial enthesopathy and rotator cuff tear. A radiologic and histologic postmortem investigation of the coracoacromial arch. Clin Orthop Relat Res 1990;(254):39-48.
33. Snyder JS. Rotator cuff: introduction, evaluation, and imaging. Shoulder arthroscopy, 2nd ed Lippincott Williams & Wilkins. 2003.
34. Oh JH, Kim JY, Lee HK, et al. Classification and clinical significance of acromial spur in rotator cuff tear: heel-type spur and rotator cuff tear. Clin Orthop Relat Res 2010;468(6):1542-1550.
35. Bigliani LU, Ticker JB, Flatow EL, et al. The relationship of acromial architecture to rotator cuff disease. Clin Sports Med 1991;10(4):823-838.
36. Tuite MJ, Toivonen DA, Orwin JF, et al. Acromial angle on radiographs of the shoulder: correlation with the impingement syndrome and rotator cuff tears. Am J Roentgenol 1995;165(3):609-613.
37. Kurtz CA, Humble BJ, Rodosky MW, Sekiya JK. Symptomatic os acromiale. J Am Acad Orthop Surg 2006;14(1):12-19.
38. Stoller DW. Magnetic Resonance Imaging in Orthopaedics and Sports Medicine. Philadelphia, PA: Lippincott Williams & Wilkins; 2007.
39. Rothenberg A, Gasbarro G, Chlebeck J, et al. The coracoacromial ligament: anatomy, function, and clinical significance. Orthop J Sports Med 2017;5(4):2325967117703398.
40. Burns WC 2nd, Whipple TL. Anatomic relationships in the shoulder impingement syndrome. Clin Orthop Relat Res 1993;(294):96-102.
41. Dong W, Goost H, Lin X-B, et al. Treatments for shoulder impingement syndrome: a PRISMA systematic review and network meta-analysis. Medicine 2015;94(10):e510.
42. Rob J. Does the addition of a corticosteroid injection to exercise therapy improve outcomes in subacromial impingement syndrome? Clin J Sport Med 2011;21(5):463-464.
43. Sachs RA, Stone ML, Devine S. Open vs. arthroscopic acromioplasty: a prospective, randomized study. Arthroscopy 1994;10(3):248-254.
44. Davis AD, Kakar S, Moros C, et al. Arthroscopic versus open acromioplasty. Am J Sports Med 2010;38(3):613-618.
45. Su W-R, Budoff JE, Luo Z-P. The effect of coracoacromial ligament excision and acromioplasty on superior and anterosuperior glenohumeral stability. Arthroscopy 2009;25(1):13-18.
46. Donigan JA, Wolf BR. Arthroscopic subacromial decompression: acromioplasty versus bursectomy alone--does it really matter? A systematic review. Iowa Orthop J 2011;31:121-126.
47. Lesko PD. Arthroscopic Mumford procedure variation of technique. Iowa Orthop J 1999;19:93-98.
48. Daluga DJ, Dobozi W. The influence of distal clavicle resection and rotator cuff repair on the effectiveness of anterior acromioplasty. Clin Orthop Relat Res 1989;(247):117-123.
49. Barbier O, Block D, Dezaly C, et al. Os acromiale, a cause of shoulder pain, not to be overlooked. Orthop Traumatol Surg Res 2013;99(4):465-472.

MRI of the Wrist

Donald von Borstel, D.O.,[1] Saya Horiuchi, M.D.,[2] Nicholas Strle, D.O.,[1] Hiroshi Yoshioka, M.D., Ph.D.[2]

[1]Department of Radiology, Oklahoma State University Medical Center, Tulsa, OK
[2]Department of Radiological Sciences, University of California, Irvine, Orange, CA

Wrist pain is a common clinical presentation and the specific diagnosis is often challenging to obtain with clinical evaluation and radiography alone. If the patient's initial radiographs are noncontributory to the diagnosis, further imaging is often necessary. MRI utilization has progressively increased due to a variety of factors, including more athletic pursuits in children that may cause wrist injury, widespread availability of MRI, and improved diagnostic capabilities of wrist MRI. Therefore, MRI is a key diagnostic modality that can heavily influence treatment decisions, making it essential that radiologists effectively diagnose common wrist disorders. This review article focuses on MRI assessment of the wrist, including ligamentous injuries, carpal fractures, and various tendon pathologies, as well as patterns of advanced collapse and avascular necrosis affecting the wrist.

Ligamentous Injury

Imaging wrist ligaments is often challenging because they are thin and have an oblique course. The wrist ligaments are commonly divided into intrinsic and extrinsic ligaments. The intrinsic ligaments attach solely to the carpal bones, whereas the extrinsic ligaments connect the ulna, radius, or metacarpals to the carpal bones.[1] They are both important for maintaining carpal stability, with intrinsic ligaments being the primary stabilizers.[2]

Intrinsic Ligaments

The scapholunate ligament (SLL) and lunotriquetral ligament (LTL) are essential for stability of the proximal carpal row.[3] For accurate injury assessment, one must be familiar with their normal variation in morphology and signal intensity.[1]

Scapholunate Ligament Injury— The SLL is horseshoe shaped with 3 components: the volar, dorsal and proximal zones. The dorsal component is approximately 3 mm thick and is associated with the joint capsule. The dorsal component is the most critical in preserving the relationship between the proximal poles of the scaphoid and the lunate.[4] The volar component is ligamentous and thinner than the dorsal component. The proximal component is the weakest and most susceptible to degenerative perforation.

MRI or MR arthrography (MRA) is of great importance in assessing the SLL. On axial images, the dorsal component is a thick, band-like structure with low signal intensity, whereas the volar component is heterogeneous (**Figure 1**). The proximal zone is best seen on coronal images. Although the proximal component of the SLL has a relatively similar triangular shape, it has a wide variety in shape (**Figure 2**). Isolated asymptomatic proximal defects are common in adults.[2] Tears of the SLL are diagnosed on MRI with findings of irregular morphology, abnormal signal intensity, and fluid transecting the ligaments.[1] A meta-analysis of the major diagnostic accuracy studies reported that the overall sensitivity and specificity of 3T-MRI for SLL tears were 75.5% and 97.1%, respectively. The sensitivity and specificity of MRA were reported as 82.1% and 92.8%, respectively.[5]

Scapholunate dissociation does not occur with disruption of the dorsal component of the SLL alone. Rather, the SLL injury in combination with injury to portions of the dorsal and volar extrinsic ligaments results in the dorsiflexed intercalated segment instability (DISI) deformity with flexion of the scaphoid and extension of the lunate and triquetrum.[6]

Lunotriquetral Ligament Injury— The LTL appears V-shaped and like the SLL, consists of the volar, dorsal and proximal zones. The dorsal component is the most important in carpal stability and resistance to rotation.[4]

The volar and dorsal zones appear band-like on axial images traversing

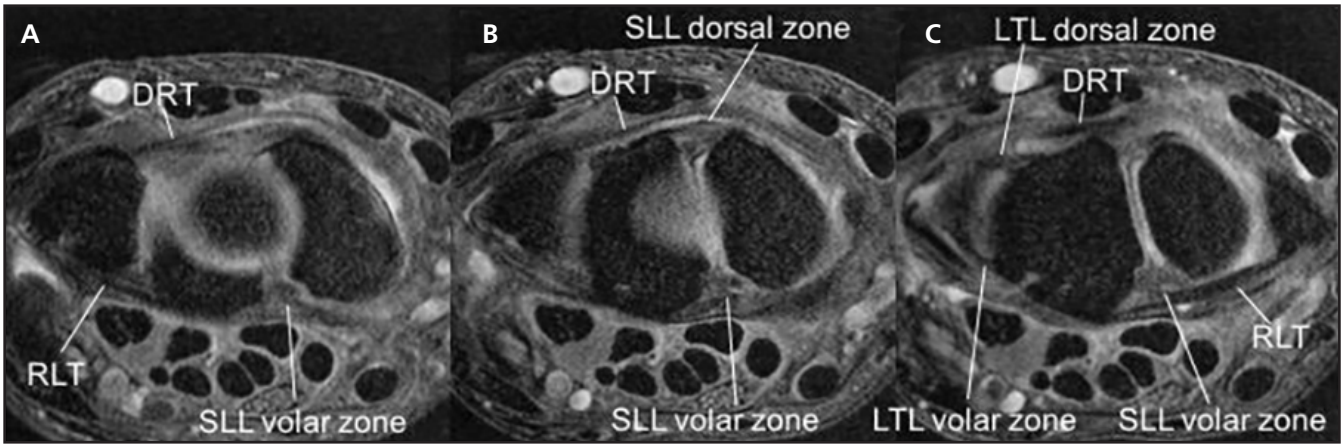

FIGURE 1. *The intrinsic and extrinsic ligaments on axial fat-suppressed (FS) proton density-weighted images (PDWI). The volar zone of the SLL shows inhomogeneous striate structure (A-C), whereas the dorsal zone of the SLL appears as a thick and band-like structure (B). The volar and dorsal zones of the LTL appear band-like and have linear shapes running in the interspace between the lunate and triquetrum (C). The RLT and DRT are hypointense band-like structures (A-C).*

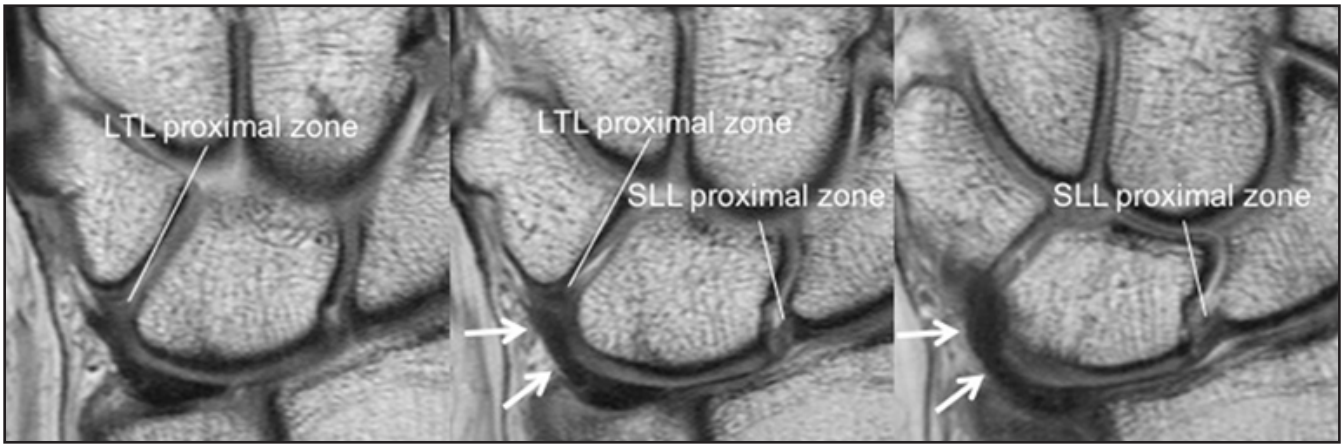

FIGURE 2. *The intrinsic ligaments on coronal PDWI. The proximal zones of the SLL and LTL show triangular shapes. Arrows show the ulnotriquetral ligament.*

between the lunate and triquetrum **(Figure 1)**. The proximal zone is best seen on coronal images with a triangular appearance **(Figure 2)**. Half of adults older than age 50 have communicating defects in the proximal zone of the LTL.[2] A few recent studies with small numbers of patients have compared the accuracy of MRI/MRA with arthroscopy. Sensitivity and specificity of MRI in detecting a complete LTL tear were 0% to 82% and 93% to 100%,[7] respectively; whereas sensitivity and specificity of MRA were 100% and 94% to 100%, respectively.[8]

LTL injuries are a common cause of ulnar-sided wrist pain and occur with a fall onto an extended, pronated, and radial deviated hand.[9] Degenerative LTL tears will result from chronic ulnar impaction syndrome.[10] Ulnar impaction syndrome is a progressive degenerative wrist condition that occurs secondary to excessive load across the ulnocarpal joint, resulting in a degenerative triangular fibrocartilage complex (TFCC) tear, disruption of the LTL, and chondromalacia of the ulna, lunate and triquetrum. Therefore, in the setting of degenerative TFCC tears, LTL lesions require careful assessment.[9]

Extrinsic Ligaments

Extrinsic ligament injuries can cause carpal instability and chronic wrist pain, especially when combined with intrinsic ligament injuries. An MR study of wrist trauma showed that 75% of patients had extrinsic ligament injuries, 60% had intrinsic ligament injuries, and almost half had combined ligamentous injuries.[11] Early ligament studies focused on only volar extrinsic ligaments; however, there is mounting evidence that both volar and dorsal capsular ligaments contribute to carpal function and alignment.[2]

Volar Extrinsic Ligaments— There are 3 major volar extrinsic ligaments: the radioscaphocapitate (RSC), radiolunotriquetral (RLT), and short radiolunate (SRL) ligaments (**Figure 3**). The RSC arises from the radial styloid process volar surface, supports the scaphoid waist, and inserts to the capitate. The RSC supports scaphoid stability acting as a "seat belt" at the scaphoid waist.[2] The RLT arises from the radial styloid process volar rim, passes volar to the proximal scaphoid pole, attaches to the volar surface of the lunate, and inserts onto the triquetrum.[2]

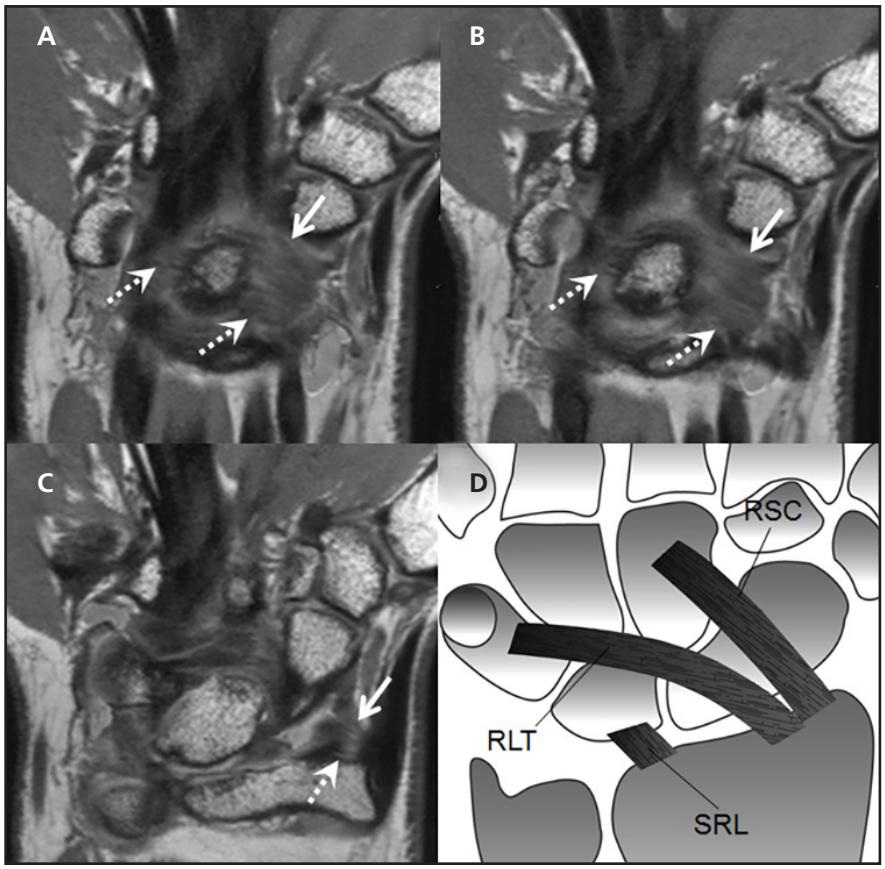

FIGURE 3. *The volar extrinsic ligaments on coronal isotropic 3D PDWI (A, B, C) and a diagram of the volar extrinsic ligaments (D): RSC (solid arrows), RLT (dashed arrows), and SRL ligaments. Both RSC and RLT show a striated appearance (A-C).*

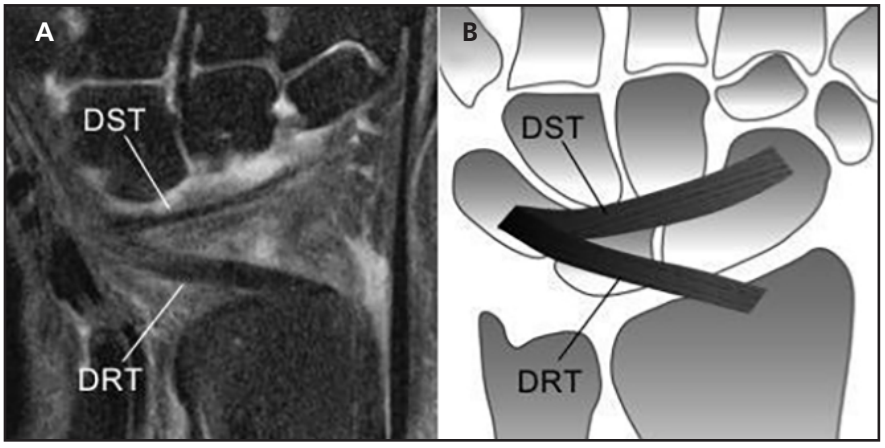

FIGURE 4. *The dorsal carpal ligaments on a coronal FS PDWI (A) and a diagram of the dorsal ligaments (B): the DRT and DST ligaments form a V-shape with the apex pointed toward the triquetrum.*

The RLT is clinically important for load transference and preventing ulnar translation of the carpus.[2] The SRL arises from the volar-ulnar aspect of the radius and attaches to the volar aspect of the lunate. Therefore, both RLT and SRL strongly anchor the lunate to the radius.

The normal RSC and RLT can be identified as linear hypointense structures with striated bands of intermediate signal intensity (**Figure 3**), whereas the SRL appears as a homogeneously hypointense focal thickening of the volar joint capsule. In the setting of trauma, the most frequently injured extrinsic ligaments were the RLT and RSC, almost half of which were associated with scaphoid injury.[11]

Dorsal Extrinsic Ligaments— Two major dorsal ligaments provide radioscaphoid stability—the dorsal radiotriquetral (DRT) and dorsal scaphotriquetral (DST) ligaments **(Figure 4)**. These ligaments form a V-shape with the apex to the triquetrum, and can be identified as linear hypointense structures, often with striated bands of intermediate signal intensity **(Figure 4)**.[2] The DRT was shown to be the third most frequently injured extrinsic ligament, and is commonly involved in triquetrum avulsions.[11]

Triangular Fibrocartilage Complex (TFCC)

The TFCC is a fibrocartilage-ligament complex providing stability to the distal radioulnar joint and helps transmit axial load from the carpus to the ulna. The TFCC is an essential pivot point for forearm rotation and is highly prone to injuries.[12] The TFCC is comprised of an articular disc (TFC disc proper) and surrounding fibrous structures—the triangular ligament, the volar and dorsal radioulnar ligaments, the ulnolunate ligament, the ulnotriquetral ligament, the ulnar collateral ligament, and the meniscus homologue **(Figure 5)**.[13] The triangular ligament has V-shaped collagen fiber bundles, which anchor the fibrocartilaginous disc proper to the tip and fovea/base of the ulnar styloid process. The volar and dorsal radioulnar ligaments form the volar and dorsal margins of the TFCC. The volar radioulnar ligament is reinforced by ulnolunate and ulnotriquetral ligaments inserting to the volar lunate and triquetrum, respectively. Although the structural terminology is still controversial, the extensor carpi ulnaris (ECU) tendon subsheath can be included as a stabilizer of the ulnar side of the TFCC. The ECU tendon changes in position between supination and pronation.[14]

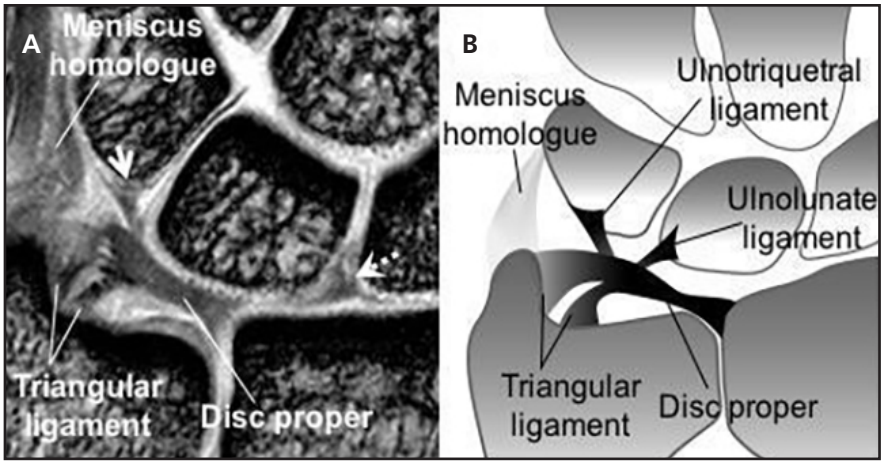

FIGURE 5. *TFCC on a coronal gradient echo T2-weighted image (A) and a diagram of the TFCC (B). The image was obtained using a 47-mm microscopy coil. The normal disc proper shows asymmetric bowtie-like low signal intensity, whereas the triangular ligament shows a striated pattern of increased internal signal. The meniscus homologue arises from the tip of the ulnar styloid process, and attaches to the ulnar side of the triquetrum and lunate. Dotted arrow shows the proximal zone of the SLL. Solid arrow shows the LTL.*

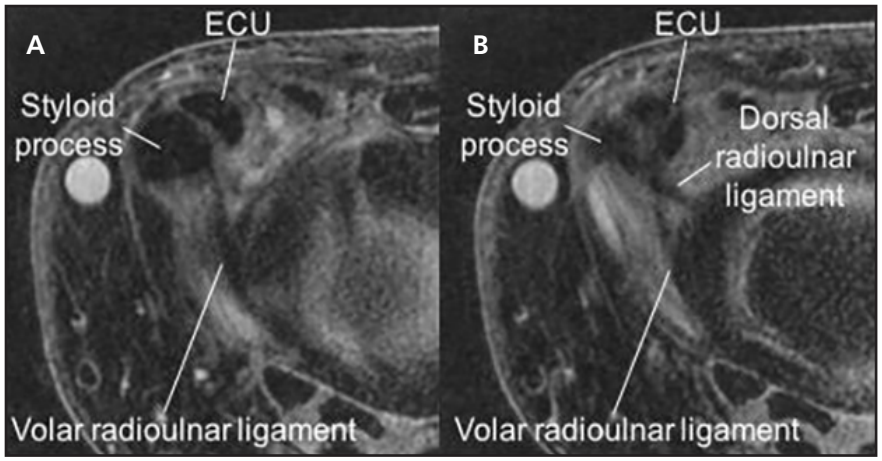

FIGURE 6*. The TFCC in neutral position on axial FS PDWI (A and B). The volar and dorsal radioulnar ligaments show hypointense band-like structures. In neutral position, the ECU tendon travels dorsally and medially to the ulnar styloid process.*

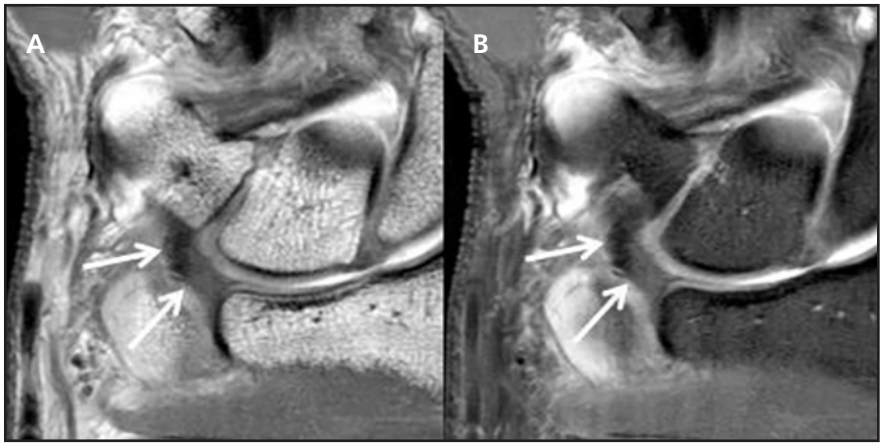

FIGURE 7. *The ulnotriquetral ligament on a coronal PDWI (A) and a coronal FS PDWI (B). The ulnotriquetral ligament arises from the disc proper and inserts to the volar surface of the triquetrum (arrows).*

On coronal images, the normal disc proper shows asymmetric bowtie-like low signal intensity, whereas the triangular ligament shows a striated pattern of increased internal signal (**Figure 5**).[15] On axial images, the volar and dorsal radioulnar ligaments are well recognized as hypointense band-like structures **(Figure 6)**. The ulnolunate and ulnotriquetral ligaments show homogeneous low-signal intensity **(Figure 7)**.

Noncontrast MRI studies have shown that the overall sensitivity and specificity for TFCC injuries were 83% and 82%, respectively.[16] MRA was superior to noncontrast MRI in an investigation of TFCC injuries, with an overall sensitivity of 84% and specificity of 95%.[17]

MR Technique for Evaluation of the TFCC

Appropriate MRI techniques should be applied for visualization of precise TFCC anatomy. **Table 1** shows a detailed overview of the typical routine sequence protocols for 3T-imaging of the wrist.[14] Images have commonly been acquired with conventional 2-dimensional (2D) techniques; however, 3D-imaging techniques reduce partial volume artifact and can be reformatted into any cross-sectional plane from a single acquisition. Although the isotropic 3D fast spin echo (FSE) sequences suffer from relatively long acquisition time and image blurring, several advanced techniques—such as parallel imaging, short TR sequences combined with driven equilibrium, and compressed sensing—have shortened overall scan time.[18]

Traumatic TFCC Tears

The Palmer classification divides TFCC tears into traumatic and degenerative lesions **(Table 2)**.[19] This classification system is frequently used by hand surgeons to guide management.[13]

Traumatic tears occur far less frequently than degenerative tears. The most common mechanism of traumatic TFCC injury is a fall on an outstretched

Table 1. Routine MR Parameters for 3T Imaging of the Wrist[14]

Sequence	Cor 3D PD FS	Cor PD	Cor PD FS	Ax PD	Ax PDFS/ Ax T_2FS	Sag PD	Sag PD FS
Pixel size (mm × mm)	0.35 × 0.35	0.27 × 0.35	0.30 × 0.32	0.4 × 0.4	0.32 × 0.44	0.40 × 0.51	0.23 × 0.32
Slice thickness (mm)	0.35	2	2	2	2	3	3
Slice gap (mm)	0	0.2	0.2	0.2	0.2	0.3	0.3
Number of slices	151	22	22	30	30	22	20-30
FOV (mm)	70	90	90	80	80	70-80	70-80
TE (ms)	29-37	30	27	30	30/70	30	27
TR (ms)	1250-1400	3500	2500-3500	2500	3000/3200	3000	2500-3500
BW (Hz/pixel)	362	194	222	250	153/218	354	175
Echo train length	70-88	13	13	9	11	12	13
NEX	2	1	3	2	2	1	1
Acquisition time (min)	~5	~2.5	~4	~3	~2.5/3	~2.8	~3.5

Key: Ax = axial; Cor = coronal; Sag = sagittal; 3D = 3-dimensional; PD = proton-density; FS = fat-suppression; FOV = field-of-view; TE = echo time; TR = repetition time; BW = bandwidth; NEX = number of excitations
Table 1 from reference 14, reproduced with permission.

Table 2. Palmer Injury Classification for the TFCC

Class I (Traumatic)
- A. Central perforation
- B. Ulnar avulsion
- C. Distal avulsion
- D. Radial avulsion

Class II (Degenerative)
- A. TFCC wear
- B. TFCC wear with lunate and/or ulnar chondromalacia
- C. TFCC perforation with lunate and/or ulnar chondromalacia
- D. C and LTL perforation
- E. D and ulnocarpal arthritis

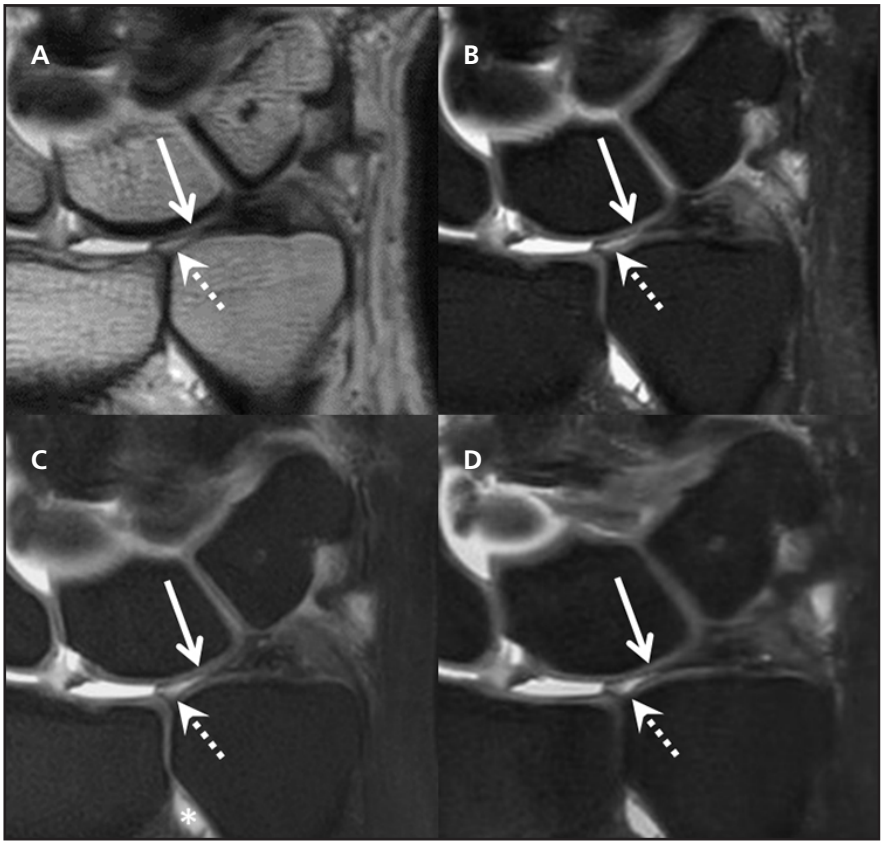

FIGURE 8. *Class IA and ID traumatic lesions of the TFCC on MR arthrogram with axial PDWI (A), FS PDWI (B), FS T1-weighted image (T1WI) (C), and isotropic 3D FS PDWI (D). There is an extensive tear of the central disc proper (solid arrow) and avulsion of the radial attachment (dashed arrows). Contrast is seen leaking through the distal radioulnar joint (asterisk image C). Class IA is the most common subtype of TFCC traumatic tears.*

hand. TFCC tears usually present clinically as ulnar-sided wrist pain and/or distal radioulnar joint instability.

Class I/traumatic TFCC tears are subclassified according to injury location. Conservative treatments are generally recommended; when conservative management is unsuccessful, several surgical options can be considered. The surgical treatments can be based on the TFCC lesion location. Class IA tear is at the central/paracentral region of the disc proper, which is the most common traumatic subtype of TFCC tears (**Figure 8**). Since the avascular central articular disc has limited healing capacity, debridement is usually performed for pain relief.[20] Class 1B tear is the avulsion of the triangular ligament with or without an ulnar styloid fracture (**Figure 9**). The instability of the distal radioulnar joint is most remarkable in Class IB injuries. Class IC tear is avulsion of the ulnolunate or ulnotriquetral ligaments, which can result in ulnocarpal instability. For Class IB and IC injuries, surgical repair may be indicated.[20] A Class ID tear involves either an avulsion tear of the

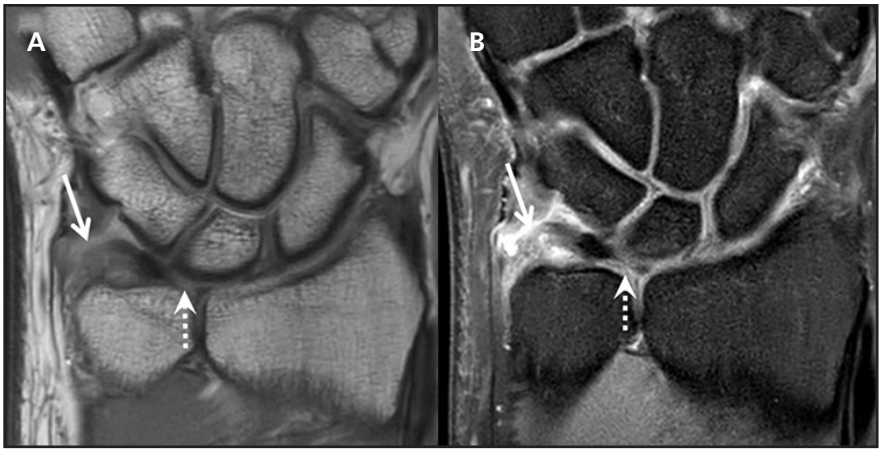

FIGURE 9. *Class IB traumatic lesion of the TFCC. PDWI (A) shows an ulnar styloid triangular ligament tear (solid arrow). FS PDWI (B) shows the hyperintense signal of the triangular ligament tear (arrow). Class IB tears involve avulsion of the triangular ligament and can occur with or without a styloid process fracture. An incidental perforation of the central disc is consistent with a concomitant Class IA lesion (dashed arrow in A and B).*

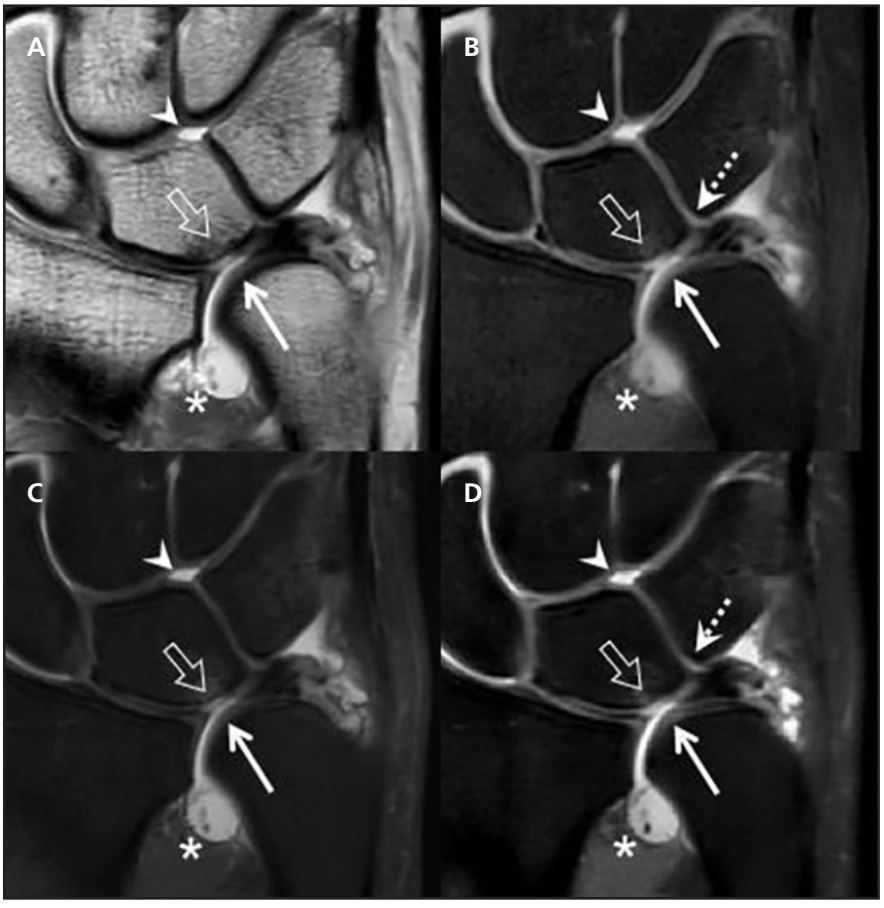

FIGURE 10. *Degeneration with perforation of the central disc of the TFCC, chondromalacia of the lunate, and LTL perforation (Palmer Class IID). MRA coronal PDWI (A), coronal FS T1WI (B), coronal FS PDWI (C), and isotropic 3D coronal FS PDWI (D) show perforation of the central disc (solid arrows) and a full thickness cartilage defect and subchondral bone marrow edema of the lunate (open arrows). A small and irregularly shaped LTL with oblique linear high-signal (contrast) through its proximal portion (dotted arrows) is visualized in (B) and (D), and intra-articular contrast extends into the midcarpal joint (arrowheads), suggesting the LTL perforation. The contrast material also extends into the distal radioulnar joint, suggesting the disc injury (asterisk).*

TFCC (**Figure 8**) or an avulsion fracture at the sigmoid notch of the radius. When the avulsion fracture exists, a direct repair leads to better outcomes.[20] For a Class ID tear without avulsion fracture, various surgical repairs have been reported and ulnar shortening osteotomy may relieve the axial load on the TFCC.

Degenerative TFCC Tears— Degenerative Class II TFCC lesions are subclassified with subtypes based on the progressive destruction of the TFCC and adjacent ligaments and cartilage. Class IIA lesions represent wear of the horizontal portion of the disc proper without perforation. Class IIB lesions resemble IIA lesions with additional chondromalacia of the lunate and/or ulna. Progression of the degenerative change results in perforation of the disc proper, which then is classified as Class IIC lesions. Class IID lesions represent a further advanced degenerative process with rupture of the LTL **(Figure 10)**. Class IIE lesions describe the final stages of ulnar impaction syndrome. These findings are often associated with ulnocarpal and distal radioulnar degenerative arthritis. In the chronic phase of TFCC injury, conservative treatments are initially selected and, if unsuccessful, ulnar shortening osteotomy or ulnar head resection can be considered.[20]

A cadaveric study reported that TFCC degeneration begins in the third decade, and subsequent perforations increase with age.[21] Similarly, MRI findings of degenerative TFCC lesions were seen with higher frequency in patients older than 50.[22] Traumatic and degenerative abnormalities are difficult to distinguish between and can coexist as age increases.

Carpal Fractures

Carpal fractures account for 21% of upper extremity fractures, with the proximal carpal row most frequently affected.[23] While plain film radiographs remain the initial imaging modality of choice, early MRI has proven a valuable tool for radiographically occult fractures. MRI has sensitivity and specificity rates

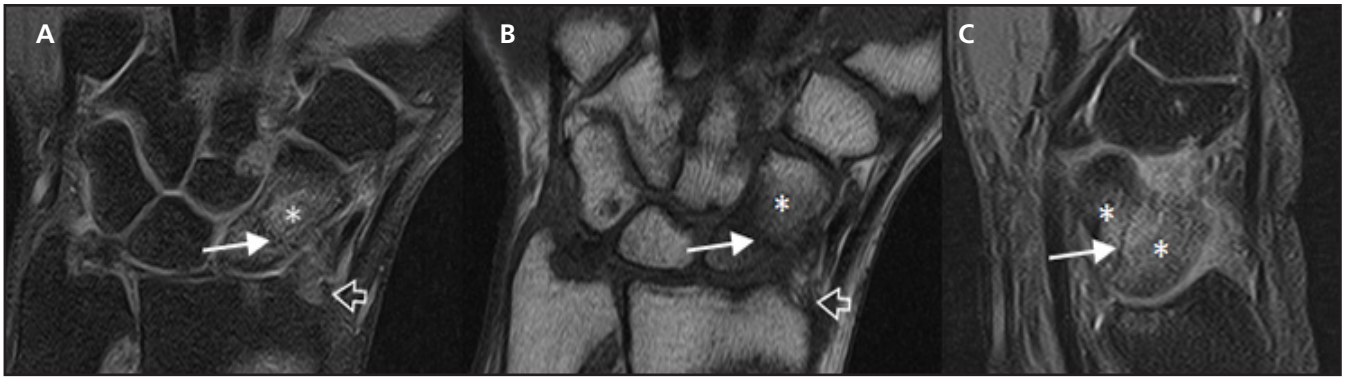

FIGURE 11. *Scaphoid fracture. Coronal FS PDWI (A) and Coronal T1WI (B) demonstrate a linear hypointense fracture line through the waist of the scaphoid (solid arrows) with adjacent reactive marrow edema (asterisks). Incidentally noted is a mildly displaced fracture of the radial styloid (open arrows). Sagittal FS PDWI (C) shows a linear hypointense fracture line through the scaphoid (solid arrow) with adjacent reactive edema (asterisks).*

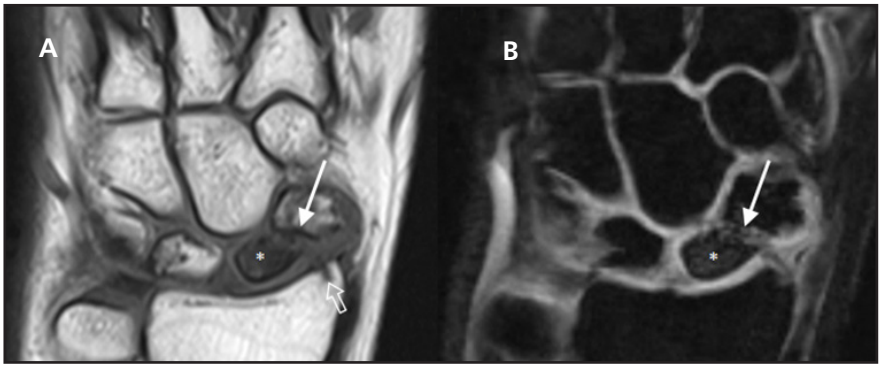

FIGURE 12. *Early scaphoid osteonecrosis. Coronal T1WI (A) shows a fracture through the waist of the scaphoid (solid arrow) with hypointense signal throughout the proximal pole (asterisk). Subtle degenerative change of the radiocarpal joint represent early scaphoid nonunion advanced collapse (SNAC wrist) (open arrow). Coronal 3D FS T2WI (B) shows a scaphoid waist fracture (solid arrow) with variable subtle increased signal throughout the proximal pole (asterisk).*

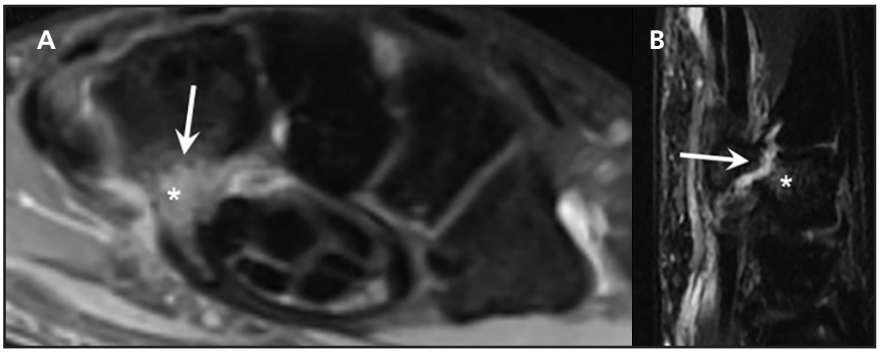

FIGURE 13. *Hamate fracture. Axial FS PDWI (A) shows fluid-like signal at the base of the hook of the hamate (solid arrow) with surrounding reactive edema (asterisk). Sagittal STIR image (B) shows linear hyperintense fracture through the base of the hook of the hamate (white arrow) with reactive edema with the body of the hamate (asterisk) and minimal displacement.*

of 80% and 100%, respectively, in radiographically occult scaphoid fractures.[24]

Carpal fractures exhibit a linear hypointensity on T1-weighted imaging (T1WI) with surrounding edema (T1-hypointensity and T2-hyperintensity). Short protocol MRI exams, consisting of short tau inversion recovery (STIR) and T1WI, have shown reliable negative predictive values in the acute setting often negating unnecessary immobilization and follow-up radiation.[25]

Scaphoid Fracture

The scaphoid is the most commonly fractured carpal bone, encompassing approximately 70% of all carpal fractures **(Figure 11)**. The scaphoid is divided into proximal, middle, and distal poles, which are important to delineate when predicting long-term healing potential. There is a single intraosseous artery (branch of the radial artery) to the scaphoid, which enters the scaphoid dorsally at the midpole (waist) and supplies the proximal pole in a retrograde fashion. While the majority of fractures heal with proper treatment, approximately 15% to 30% of scaphoid fractures will develop osteonecrosis, which increases in prevalence with proximal pole and displaced fractures.[26]

Up to 40% of scaphoid fractures are missed at initial presentation, and follow-up MRI of the wrist is becoming more common. A scaphoid fracture segment with hypointense T1- and T2-signal is concerning for decreased vascularity. While these findings alone are a poor predictor of impending osteonecrosis/nonunion, they should raise suspicion for potential setbacks in healing **(Figure 12)**.[27] As osteonecrosis develops, the scaphoid will exhibit fragmentation and collapse.

Treatment of scaphoid fractures is typically achieved conservatively with immobilization. Stable, nondisplaced fractures involving the mid/distal poles achieve a union rate of 90% with casting alone.[27] Surgery is commonly reserved for unstable or displaced fractures, proximal pole fractures, or when nonunion/osteonecrosis occurs.

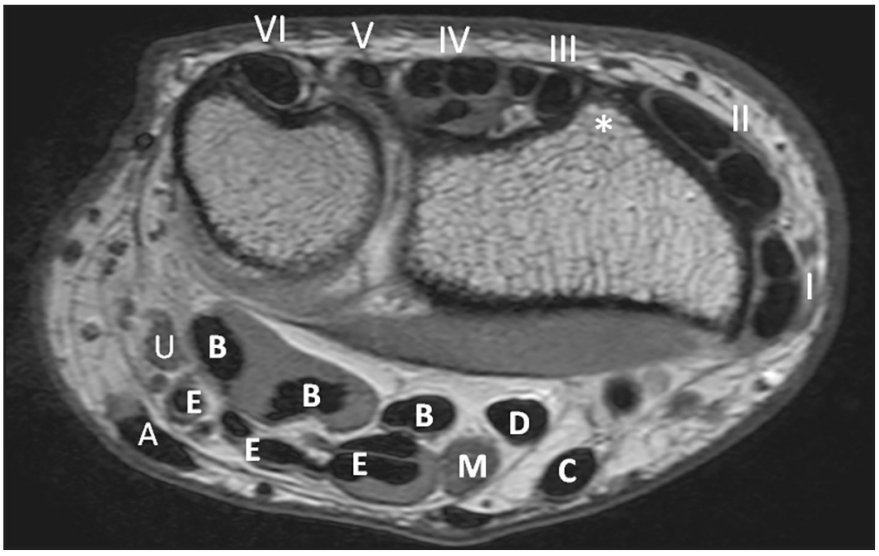

FIGURE 14. *The extensor tendon compartments and the flexor tendons. Axial PDWI displays Lister tubercle (asterisk), which serves as a landmark for the dorsal wrist. The extensor compartments are labeled with their respective Roman numerals I-VI. Extensor tendons within these compartments are: I = abductor pollicis longus and extensor pollicis brevis, II = extensor carpi radialis longus and brevis, III = extensor pollicis longus, IV = extensor digitorum and indicis, V = extensor digiti minimi, VI = extensor carpi ulnaris. The flexor tendons and the 2 nerves are also labelled and indicated in letters. A = flexor carpi ulnaris, B = flexor digitorum profundus, C = flexor carpi radialis, D = flexor pollicis longus, E = flexor digitorum superficialis, M = median nerve, U = ulnar nerve.*

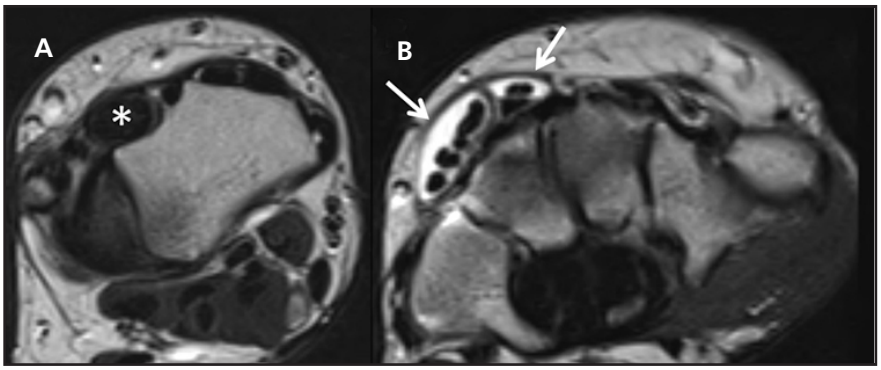

FIGURE 15. *Tendinopathy and tenosynovitis. Axial T2WI (A) shows focal thickening of the extensor compartment IV extensor digitorum and indicis tendons (asterisk), consistent with tendinopathy. Axial T2WI (B) shows fluid within the tendon sheaths of the extensor compartments III and IV (solid arrows), consistent with tenosynovitis.*

Triquetral Fracture

The triquetrum is the second-most commonly fractured carpal bone, accounting for 18.3% of carpal fractures.[28] They typically involve the dorsal cortex and are most frequently diagnosed on lateral radiographs of the wrist. Triquetral fractures are radiographically occult in up to 20% of cases.[28,29] On MRI, the most sensitive finding is bone marrow edema, which may even obscure the fracture line. Most commonly, the small fracture fragment is visualized within the dorsal soft tissues and follows the osseous signal on all sequences; however, diffuse soft-tissue edema may obscure these fragments.

It has been suggested that the dorsal fracture fragment results from a dorsal extrinsic ligament avulsion injury.[28] There is often combined ligamentous injury in these patients, which reinforces MRI's role in acute wrist injuries. Less frequent triquetral fractures involve the body of the triquetrum (typically in the setting of perilunate fracture dislocation) and volar avulsion fractures (ulnotriquetral or lunotriquetral ligament avulsion).

Hamate Fracture

Hamate fractures account for 1.7% of carpal fractures, with the hook of the hamate the most frequent site.[29] They are associated with racket sports as the handle directly compresses the protruding hook. Given the tendinous and ligamentous insertions on the hook of the hamate, associated displacement of the fragment may delay healing or nonunion. Occasionally, fractures may involve the body of the hamate, typically due to an axial loading injury or associated perilunate dislocations.[26]

MRI demonstrates a T1-hypointense and T2-hyperintense fracture line (**Figure 13**). Comment should be made on the degree of displacement and signal characteristics of the displaced fragment, as there is increased risk of nonunion when the hook of the hamate is involved.

Tendon Pathology

Normal Tendon Appearance

Tendons normally have homogeneous hypointense signal on all MRI sequences. Wrist tendons are divided into the flexor and extensor subgroups, and are best appreciated in the axial plane (**Figure 14**).[30] Most flexor tendons traverse the carpal tunnel, with 3 located outside the tunnel: the flexor carpi ulnaris, flexor carpi radialis, and the palmaris longus (PL) tendons. The PL is not present in a minority of the population. The extensor tendons are divided into 6 compartments, each with a separate tenosynovial sheath.[31]

General Tendon Abnormalities

Pathology of the wrist tendons include tendinopathy, tenosynovitis, and partial and complete tears. MRI allows the radiologist to reliably distinguish between these entities.

Tendinopathy is a generalized term describing diffuse or focal tendon thickening. This is usually secondary to chronic overuse and presents with T2-hyperintense signal within the tendon substance (**Figure 15A**).

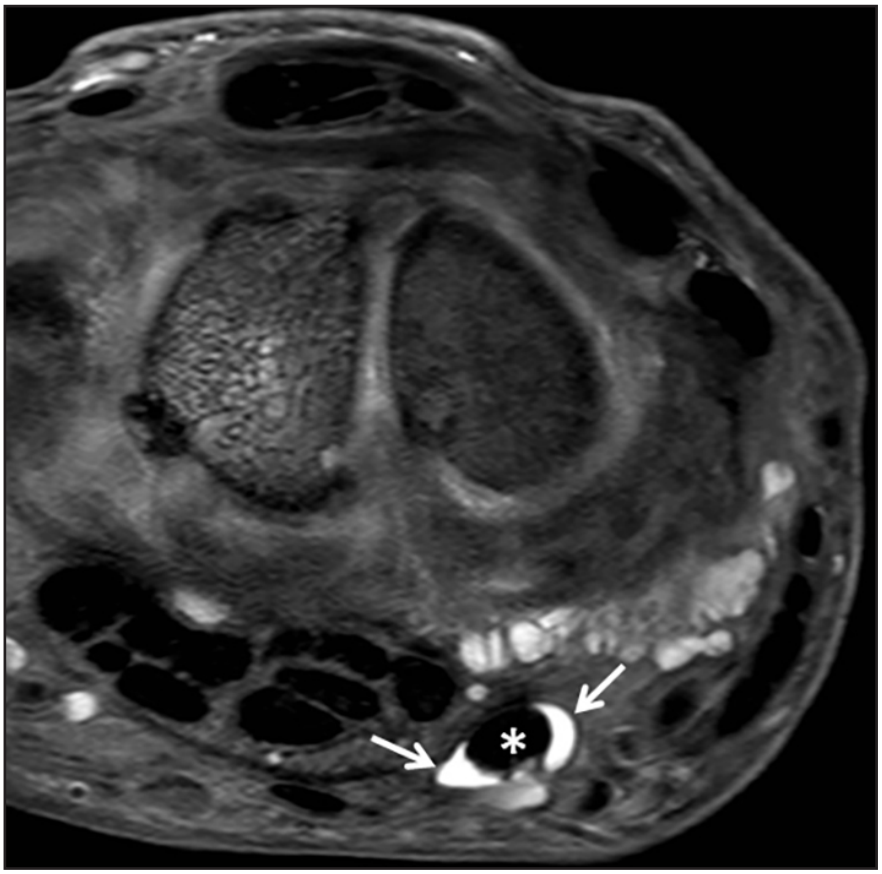

FIGURE 16. *Tenosynovitis of the flexor carpi radialis (FCR) tendon (asterisk). Axial FS PDWI displaying hyperintense fluid-like signal within the distended tendon sheath (arrows) of the FCR. The tendon sheath is distended and has an increased diameter compared to the tendon itself.*

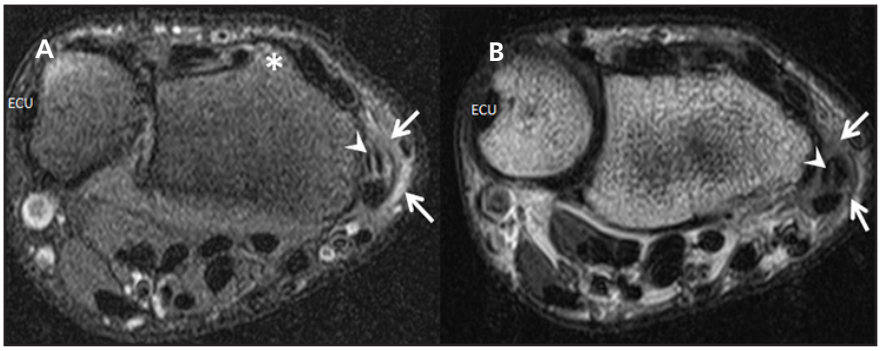

FIGURE 17. *Partial tendon tear. Axial FS PDWI (A) and axial PDWI (B) displaying interstitial hyperintense signal within the extensor pollicis brevis tendon (arrowhead). This is consistent with a partial interstitial split tear of the tendon. There is also peritendinous fluid-like signal and tendon sheath distention, consistent with de Quervain tenosynovitis (solid arrows). The anatomical landmark Lister tubercle is displayed (asterisk) as well as the extensor ECU.*

Tenosynovitis presents with a hyperintense fluid-signal within the tendon sheath **(Figures 15B, 16)**. The diameter of the tendon sheath fluid is greater than the tendon diameter. Fluid-like signal that does not surround the tendon is most commonly a normal finding. Usually patients with tenosynovitis or tendinopathy complain of localized tenderness, decreased grip strength, and pain with range of motion. These entities are usually related to repetitive trauma and inflammatory or infectious arthritis. Any wrist tendon may be affected; however, tendons at a point of restriction are most commonly involved (eg, the ECU tendon as it passes over the ulnar groove). They are often successfully treated with conservative therapy.

MRI findings of a torn tendon include a focal disruption or distorted appearance of the tendon. *Partial tears* have a focal region of hyperintense T1- and T2-signal with some fibers remaining intact **(Figure 17)**. *Complete tears* show full-thickness discontinuity at any point of the tendon and often present with retraction of the torn tendon. Peritendinous edema and/or hemorrhage suggest an acute tear. Tendon tears are often treated conservatively with splinting. However, if conservative treatment fails or the tear is > 40% thickness of the tendon, primary surgical repair is often performed.[30]

de Quervain Tenosynovitis

First described in 1895, this condition is a stenosing tenosynovitis affecting the extensor pollicis brevis (EPB) and abductor pollicis longus (APL) tendons of the wrist.[30,32,33] This results from chronic overuse and can commonly be seen in women (particularly new mothers), racquet sports, golf, and also recently recognized in frequent texters.

Patients present with pain along the radial aspect of the wrist exacerbated by thumb adduction and ulnar deviation of the wrist. There can be localized swelling and tenderness. The Finkelstein test is positive when pain occurs upon passive ulnar deviation while the thumb is adducted.

MRI displays EPB and APL tenosynovitis with fluid-like signal within the tendon sheath. Associated tendinopathy varies from localized tendon thickening to an interstitial tear. Peritendinous edema-like signal also often surrounds the first extensor compartment **(Figure 18)**.

Treatment begins conservatively with nonsteroidal anti-inflammatory drugs (NSAIDS) and immobilization with a thumb spica brace. Corticosteroid injection into the first dorsal compartment can also yield good results. Surgical decompression is reserved for patients who fail these measures.

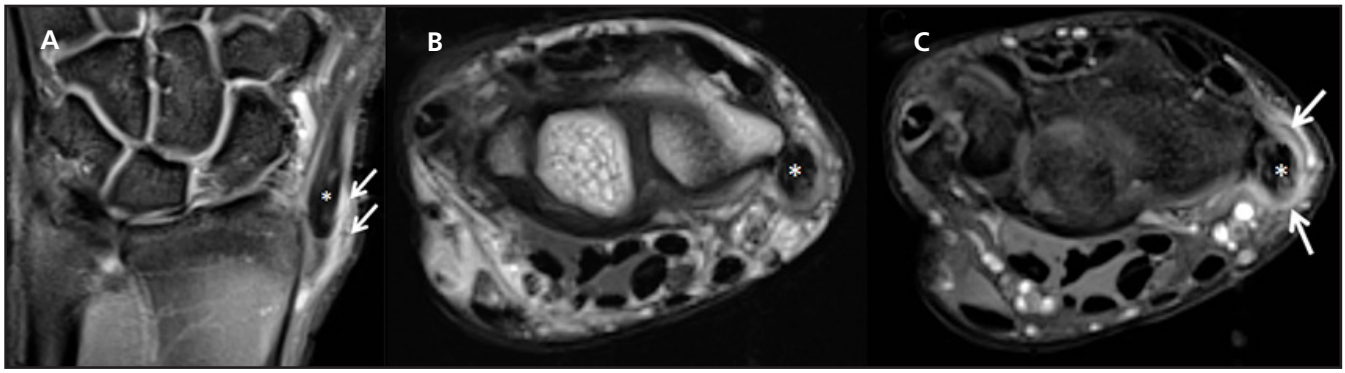

FIGURE 18. *de Quervain tenosynovitis. Coronal FS PDWI (A), axial PDWI (B), and axial FS PDWI (C) of the wrist. Fluid-like signal within the thickened extensor pollicis brevis and abductor pollicis longus tendons consistent with tendinopathy (asterisk). There is fluid within the tendon sheaths (tenosynovitis) and adjacent soft tissues (arrows).*

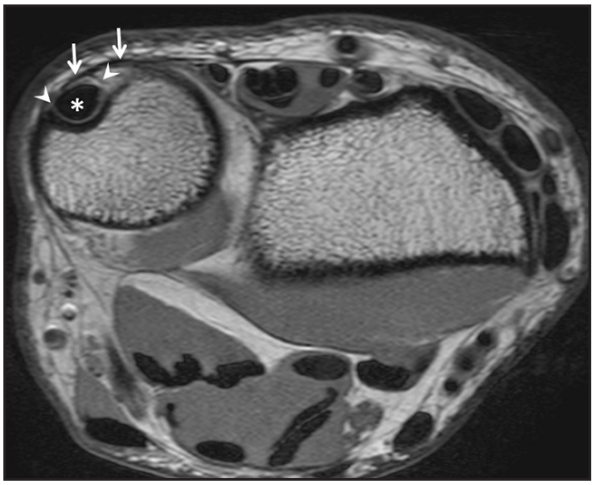

FIGURE 19. *ECU tendon. Single axial PDWI at the level of the distal ulna showing the ECU subsheath (arrowheads) deep to the overlying extensor retinaculum (solid arrows). The ECU subsheath and extensor retinaculum form the fibro-osseous tunnel for the ECU and blend together along the dorsal aspect. The normal ECU tendon is seen (asterisk) and has normal diffusely low-signal intensity.*

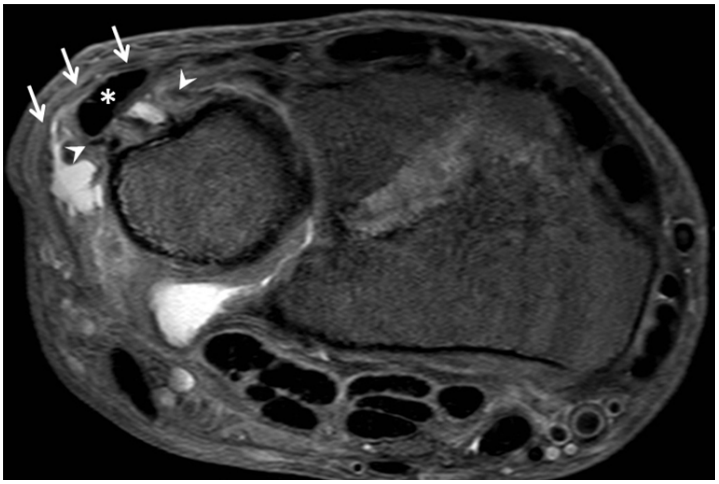

FIGURE 20*. ECU subsheath tear at both the dorsal and volar attachments with subluxation of the ECU tendon. Single axial FS PDWI demonstrating a subluxed ECU tendon (asterisk), which lies dorsal and ulnar to the disrupted subsheath (arrowheads). The subsheath is diffusely thickened and laxed in appearance with tenosynovitis present. The extensor retinaculum remains intact (solid arrows).*

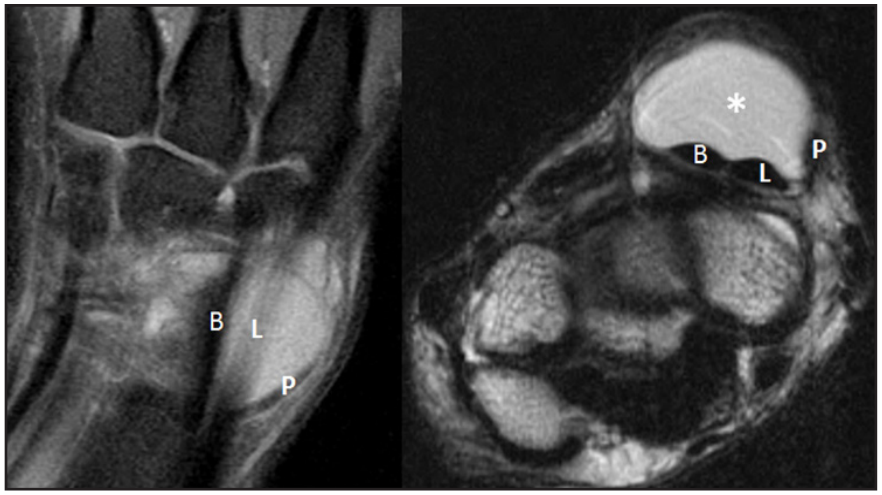

FIGURE 21. *Coronal FS PDWI (A) and axial T2WI (B) in the distal intersection syndrome of the wrist. The displaced extensor pollicis longus tendon (P) crossing over the extensor carpi radialis longus (L) and extensor carpi radialis brevis (B) tendons. The tendon sheath of L and B is markedly distended with fluid-like signal (asterisk), as there is friction between the crossing tendons.*

Extensor Carpi Ulnaris Injuries

The ECU has unique anatomical characteristics and courses along the dorsomedial aspect of the forearm through its own fibro-osseous tunnel, in a groove between the ulnar head and the styloid process.[10,14,34] This tunnel is formed by the distal ulna and a band of connective tissue known as the ECU subsheath, which stabilizes the ECU as it courses over the distal ulna **(Figure 19)**. The combination of the subsheath and extensor retinaculum prevent subluxation and friction of the ECU tendon.

Extensor Carpi Ulnaris Tenosynovitis and Tendinosis

These entities occur from repetitive stress causing synovial inflammation

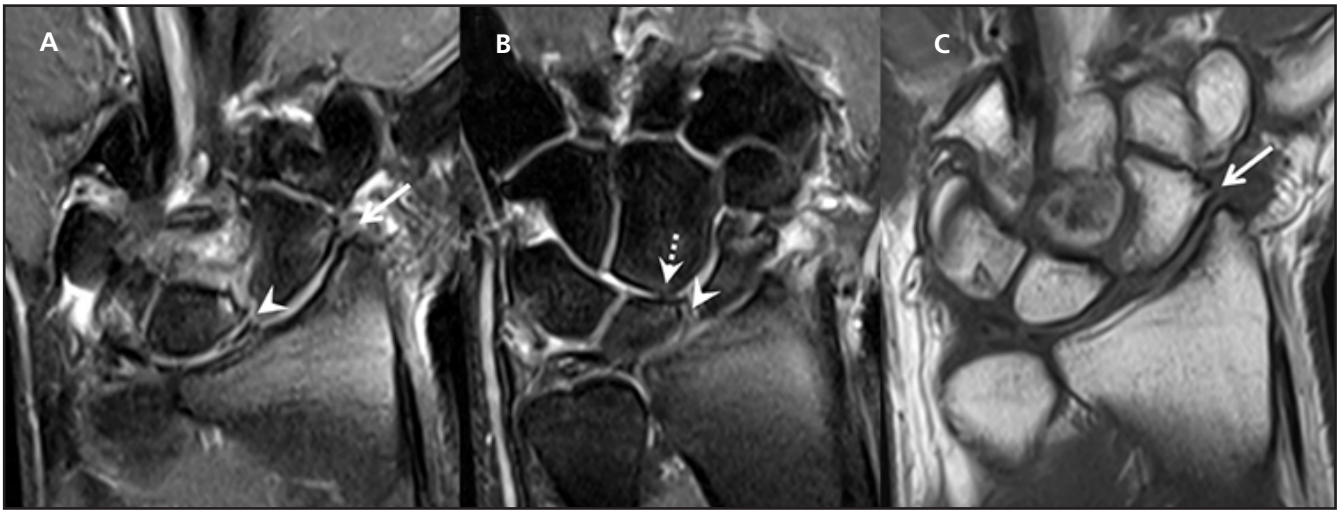

FIGURE 22. *SLAC wrist. Coronal FS PDWI (A and B) and a single coronal T1WI (C). There is a partial proximal segment tear of the SLL (arrowheads, A and B) with joint space narrowing, sclerosis, and osteophyte formation of the radioscaphoid joint. This is most significant along the radial styloid (solid arrows, A and C). There is joint space loss (dashed arrow, B) and sclerosis of the capitolunate joint, suggesting stage III disease.*

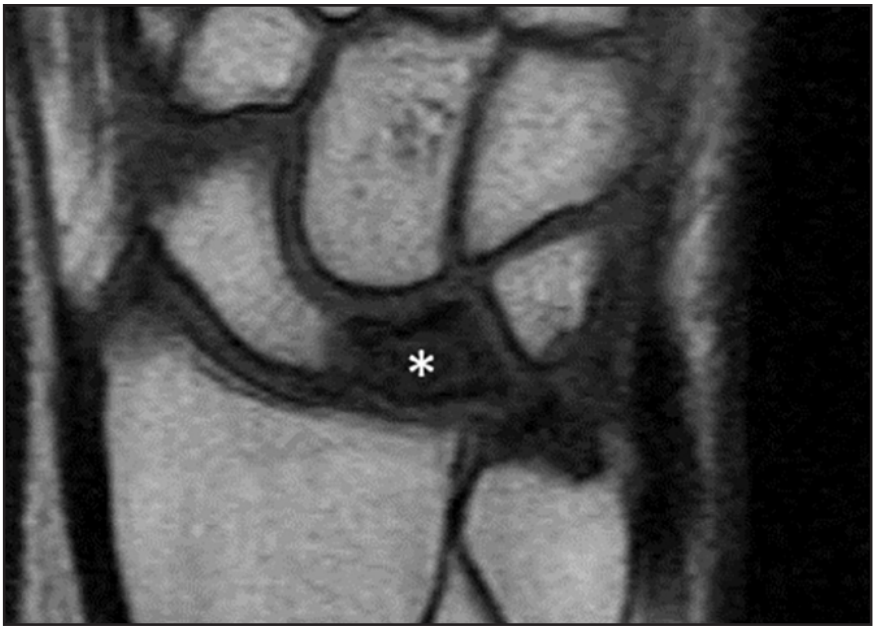

FIGURE 23. *Kienbock's disease. Coronal T1WI displays homogeneous T1-hypointensity throughout the lunate without collapse (asterisk). This is consistent with Lichtman stage II classification. This process follows a progression with stage III disease having early collapse of the lunate, and stage IV displaying continued collapse with radiocarpal and midcarpal degenerative joint disease.*

and are commonly seen in athletes, particularly rowers and racquet sport players. Typical presentation includes point tenderness and swelling at the dorsal/ulnar aspect of the wrist.

Progression usually begins with tenosynovitis and circumferential hyperintense T2-signal on MRI. Continued stress leads to tendinopathy and ultimately tendon tear.[9] A pitfall on MRI is the "pseudolesion," which is when the tendon has centrally increased T1- and T2-signal on axial images at the level of the distal radioulnar joint (DRUJ). This is secondary to intrasubstance mucoid degeneration or magic angle effect.[1,35] Nonfocal increased signal and tendon thickening distinguish true tendinosis from a pseudolesion.

Nonsurgical conservative treatment is often successful with splinting of the wrist for 6 to 8 weeks. If this fails, surgical release of the sixth compartment can be performed with tendon debridement and subsheath reconstruction.

Extensor Carpi Ulnaris Subsheath Injury

The ulnar wall of the subsheath can rupture in the setting of trauma or with recurrent stress injuries. This often results in ECU subluxation, with ulnar displacement of the tendon, even if the overlying extensor retinaculum is intact.[9,30] The tendon commonly returns to a normal position in pronation. On MRI, the ECU is subluxed with complete tears of the ECU subsheath dorsal attachment. The volar attachment of the ECU subsheath is often lax and there is usually peritendinous edema **(Figure 20)**.

Intersection Syndrome

There are 2 intersection syndromes involving the extensor tendons second compartment.[31,36] The *distal intersection syndrome* involves the extensor pollicis longus (EPL) as it crosses over the extensor carpi radialis longus (ECRL) and extensor carpi radialis brevis (ECRB) tendons, and is rare **(Figure 21)**. The more common *proximal intersection syndrome* involves the APL and EPB myotendinous junctions as they cross over the ECRL and ECRB. This occurs approximately 4 to 8 cm

proximal to the Lister tubercle and is known as the "oarsmen's wrist," commonly affecting rowers and weightlifters as a result of repetitive wrist flexion/extension. MRI shows tenosynovitis involving the tendon with surrounding soft-tissue, edema-like signal.[36]

These intersection syndromes are commonly treated conservatively with steroid or local anesthetic injection into the second compartment. If this fails, tenosynovectomy and decompression can be performed at the level of intersection.

Scapholunate Advanced Collapse (SLAC) and Scaphoid Nonunion Advanced Collapse (SNAC)

These entities represent the most common types of wrist arthritis seen by hand surgeons.[37] Given their prevalence and associated disability, it is important to recognize them radiographically. MRI is unnecessary for staging the disease, but displays cartilage to a much better extent.[38]

SLAC wrist pattern of osteoarthritis occurs after injury or degenerative attenuation of the SLL. SNAC wrist develops following a scaphoid fracture that progresses to nonunion. There is a traditional 4-stage classification scheme of SLAC and SNAC wrists.[39] Stage I displays arthrosis at the radial styloid-distal scaphoid articulation. Stage II involves the proximal radioscaphoid joint in SLAC wrists and the scaphocapitate joint in SNAC wrists. Stage III involves degeneration of the midcarpal joint, and specifically the capitolunate joint **(Figure 22)**. Stage IV involves pancarpal arthrosis with preservation of the radiolunate joint.

Kienbock disease

Kienbock disease is avascular necrosis of the lunate (lunatomalacia or lunate osteonecrosis). The most common theory for this entity is compromise of the lunate vasculature.[40] Risk factors associated with Kienbock disease include negative ulnar variance, high uncovering of the lunate, abnormal radial inclination, and trapezoidal shape of the lunate.[41] Without prompt diagnosis and treatment, disease progression will ultimately lead to joint destruction within 3 to 5 years.[40]

The pattern of disease follows a progression delineated by the Lichtman classification, staging by lunate morphology and signal characteristics **(Figure 23)**. In *stage I*, the lunate maintains its normal morphology, but develops a uniform edema-like pattern of diffuse T1-weighted hypointensity and hyperintense signal on fluid-sensitive sequences. *Stage II* denotes the early sclerotic changes of the lunate with hypointense signal on T1WI and variable signal on fluid-sensitive sequences. Stage II also marks the earliest findings on plain film radiography with increased density of the lunate. Progression to collapse is first demonstrated in *stage III* with loss of height in the coronal plane and lengthening of the lunate in the sagittal plane. *Stage IV* is characterized by lunate collapse along with radiocarpal and midcarpal degenerative change. In addition, an adjacent reactive synovitis and joint effusion may be associated.[40] If intravenous gadolinium is used during imaging, nonenhancing portions of the lunate are concerning for nonviable fragments, although late revascularization may occur.

Conclusion

MRI of the wrist is progressively increasing in utilization, but is often a daunting task for interpreting radiologists. Understanding the complex anatomy of the wrist and more common disease of the ligamentous, osseous, and tendinous structures allows the radiologist to efficiently and accurately evaluate MRI of the wrist with improved diagnostic capabilities. This ultimately leads to more efficient treatment and better patient outcomes.

References

1.Burns JE, Tanaka T, Ueno T, et al. Pitfalls that may mimic injuries of the triangular fibrocartilage and proximal intrinsic wrist ligaments at MR imaging. Radiographics 2011;31(1):63-78.

2.Ringler MD, Murthy NS. MR Imaging of wrist ligaments. Magn Reson Imaging Clin N Am 2015;23(3):367-391.

3.Tanaka T, Ogino S, Yoshioka H. Ligamentous injuries of the wrist. Semin Musculoskelet Radiol 2008;12(4):359-377.

4.Bateni CP, Bartolotta RJ, Richardson ML, et al. Imaging key wrist ligaments: what the surgeon needs the radiologist to know. Am J Roentgenol 2013;200(5):1089-1095.

5.Hafezi-Nejad N, Carrino JA, Eng J, et al. Scapholunate interosseous ligament tears: diagnostic performance of 1.5 T, 3 T MRI, and MR arthrography—a systematic review and meta-analysis. Acad Radiol 2016;23(9):1091-1103.

6.Elsaftawy A, Jabłecki J, Jurek T, et al. New concept of scapholunate dissociation treatment and novel modification of Brunelli procedure—anatomical study. BMC Musculoskelet Disord 2014;15:172.

7.Magee T. Comparison of 3-T MRI and arthroscopy of intrinsic wrist ligament and TFCC tears. Am J Roentgenol 2009;192(1):80-85.

8.Asaad AM, Andronic A, Newby MP, et al. Diagnostic accuracy of single-compartment magnetic resonance arthrography in detecting common causes of chronic wrist pain. J Hand Surg Eur Vol 2017;42(6):580-585.

9.Watanabe A, Souza F, Vezeridis PS, et al. Ulnar-sided wrist pain. II. Clinical imaging and treatment. Skeletal Radiol 2010;39(9):837-857.

10. Vezeridis PS, Yoshioka H, Han R, et al. Ulnar-sided wrist pain. Part I: anatomy and physical examination. Skeletal Radiol 2010;39(8):733-745.

11. Taneja AK, Bredella MA, Chang CY, et al. Extrinsic wrist ligaments: prevalence of injury by magnetic resonance imaging and association with intrinsic ligament tears. J Comput Assist Tomogr 2013;37(5):783-789.

12. Kirchberger MC, Unglaub F, Mühldorfer-Fodor M, et al. Update TFCC: histology and pathology, classification, examination and diagnostics. Arch Orthop Trauma Surg 2015;135(3):427-437.

13. Cody ME, Nakamura DT, Small KM, et al. MR Imaging of the triangular fibrocartilage complex. Magn Reson Imaging Clin N Am 2015;23(3):393-403.

14. von Borstel D, Wang M, Small K, et al. High-resolution 3T MR Imaging of the triangular fibrocartilage complex. Magn Reson Med Sci 2017;16(1):3-15.

15. Yoshioka H, Burns JE. Magnetic resonance imaging of triangular fibrocartilage. J Magn Reson Imaging 2012;35(4):764-778.

16. Wang ZX, Chen SL, Wang QQ, et al. The performance of magnetic resonance imaging in the detection of triangular fibrocartilage complex injury: a meta-analysis. J Hand Surg Eur Vol 2015;40(5):477-484.

17. Smith TO, Drew B, Toms AP, et al. Diagnostic accuracy of magnetic resonance imaging and magnetic resonance arthrography for triangular fibrocartilaginous complex injury: a systematic review and meta-analysis. J Bone Joint Surg Am 2012;94(9):824.

18. Chang AL, Yu HJ, von Borstel D, et al. Advanced imaging techniques of the wrist. Am J Roentgenol 2017;209(3):497-510.

19. Palmer AK. Triangular fibrocartilage complex lesions: a classification. J Hand Surg Am 1989;14(4):594-606.

20. Minami A. Triangular fibrocartilage complex tears. Hand Surg 2015;20(1):1-9.

21. MikićZD. Age changes in the triangular fibrocartilage of the wrist joint. J Anat 1978;126(Pt 2):367-384.

22. Nozaki T, Rafijah G, Yang L, et al. High-resolution 3 T MRI of traumatic and degenerative triangular fibrocartilage complex (TFCC) abnormalities using Palmer and Outerbridge classifications. Clin Radiol 2017;72(10):904.e1-e904.e10.
23. Ootes D, Lambers KT, Ring DC. The epidemiology of upper extremity injuries presenting to the emergency department in the United States. Hand 2012;7(1):18-22.
24. Beeres FJP, Rhemrev SJ, den Hollander P, et al. Early magnetic resonance imaging compared with bone scintigraphy in suspected scaphoid fractures. J Bone Joint Surg Br 2008;90(9):1205-1209.
25. Kanavaki A, Draenert C, Ceroni D, et al. Short MRI protocol for excluding traumatic lesions of the scaphoid bone in children. In Vivo 2016;30(4):495-499.
26. Kaewlai R, Avery LL, Asrani AV, et al. Multidetector CT of carpal injuries: anatomy, fractures, and fracture-dislocations. Radiographics 2008;28(6):1771-1784.
27. Dawson JS, Martel AL, Davis TR. Scaphoid blood flow and acute fracture healing. A dynamic MRI study with enhancement with gadolinium. J Bone Joint Surg Br 2001;83(6):809-814.
28. Becce F, Theumann N, Bollmann C, et al. Dorsal fractures of the triquetrum: MRI findings with an emphasis on dorsal carpal ligament injuries. Am J Roentgenol 2013;200(3):608-617.
29. Welling RD, Jacobson JA, Jamadar DA, et al. MDCT and radiography of wrist fractures: radiographic sensitivity and fracture patterns. Am J Roentgenol 2008;190(1):10-16.
30. Plotkin B, Sampath SC, Sampath SC, et al. MR imaging and US of the wrist tendons. Radiographics 2016;36(6):1688-1700.
31. Meraj S, Gyftopoulos S, Nellans K, et al. MRI of the extensor tendons of the wrist. Am J Roentgenol 2017;209(5):1093-1102.
32. Lok RLK, Griffith JF, Ng AWH, et al. Imaging of radial wrist pain. Part II: pathology. Skeletal Radiol 2014;43(6):725-743.
33. Cockenpot E, Lefebvre G, Demondion X, et al. Imaging of sports-related hand and wrist injuries: sports imaging series. Radiology 2016;279(3):674-692.
34. Henderson CJ, Kobayashi KM. Ulnar-sided wrist pain in the athlete. Orthop Clin North Am 2016;47(4):789-798.
35. Ali S, Cunningham R, Amin M, et al. The extensor carpi ulnaris pseudolesion: evaluation with microCT, histology, and MRI. Skeletal Radiol 2015;44(12):1735-1743.
36. de Lima JE, Kim H-J, Albertotti F, et al. Intersection syndrome: MR imaging with anatomic comparison of the distal forearm. Skeletal Radiol 2004;33(11):627-631.
37. Watson HK, Ballet FL. The SLAC wrist: scapholunate advanced collapse pattern of degenerative arthritis. J Hand Surg Am 1984;9(3):358-365.
38. Li AE, Lee SK, Rancy SK, et al. Comparison of Magnetic Resonance Imaging and Radiographs for Evaluation of Carpal Osteoarthritis. J Wrist Surg 2017;6(2):120-125.
39. Shah CM, Stern PJ. Scapholunate advanced collapse (SLAC) and scaphoid nonunion advanced collapse (SNAC) wrist arthritis. Curr Rev Musculoskelet Med 2013;6(1):9-17.
40. Arnaiz J, Piedra T, Cerezal L, et al. Imaging of Kienböck disease. Am J Roentgenol 2014;203(1):131-139.
41. Lutsky K, Beredjiklian PK. Kienböck Disease. J Hand Surg Am 2012;37(9):1942-1952.

Intermetatarsal Lesion

Jeff Lee, D.O., Timothy McCay, D.O., Donald von Borstel, D.O.

Department of Radiology, Oklahoma State University Medical Center, Tulsa, OK

Case Presentation

A 44-year-old woman presented with a 2-year atraumatic history of right forefoot pain. Past medical history and review of systems were noncontributory. She complained of worsening pain with ambulation and physical activity, with pain centered over the forefoot. The clinician was primarily concerned about a metatarsal stress fracture upon physical examination. Initial foot radiographs were normal, leading to further evaluation with MRI (**Figures 1A-D**).

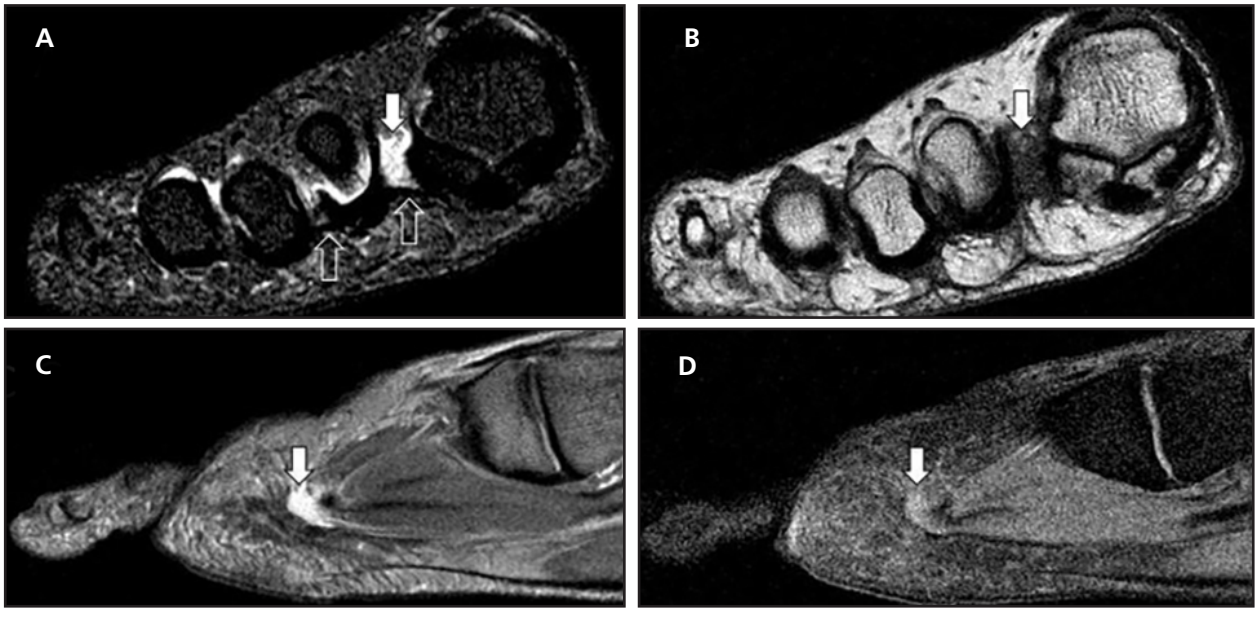

FIGURE 1. *Coronal short tau inversion recovery (STIR) (A), coronal T1 (B), sagittal STIR (C), and sagittal fat-suppressed postcontrast T1 (D) images of the right forefoot demonstrate a STIR hyperintense and T1 hypointense lesion (solid arrows) within the first intermetatarsal space. The lesion lies entirely above the deep transverse metatarsal ligament (open arrows). The lesion is iso- to slightly hyperintense compared with adjacent musculature on the postcontrast image (D) indicating no or minimal enhancement.*

Key Imaging Finding

First intermetatarsal space lesion

Differential Diagnosis

Stress fracture
Morton neuroma
Intermetatarsal bursitis
Ganglion cyst
Abscess (osteomyelitis)
Schwannoma

Discussion

Forefoot pain is a common symptom encountered by clinicians. The forefoot is the major site of load bearing during ambulation and undergoes additional stress with running or jumping motion.[1] As a result, a wide range of patients from elite athletes to the elderly can present with this symptomatology.

The forefoot contains many intricate support structures and, consequently, a myriad of sources can lead to pain in this region.[2] These can be categorized into trauma, infection, arthropathy, tendon disorders, and neoplastic and non-neoplastic masses.

Traumatic lesions such as metatarsal stress fractures or capsuloligamentous injuries (ie, turf toe) are commonly seen in athletes or active individuals such as military recruits. Patients with diabetes or other neuropathic processes frequently develop osteomyelitis and septic joint due to transcutaneous spread of infection from overlying ulcers. Degenerative joint disease is the most common arthropathy affecting the forefoot; however, other etiologies such as rheumatoid arthritis and gout often affect the metatarsal region with accompanying soft-tissue sequelae (ie, pannus and tophus). Tendon disorders such as tendinosis and tenosynovitis are commonly post-traumatic in nature; however, the etiology is often multifactorial with contributing systemic diseases or underlying infection. Many osseous and soft-tissue masses may cause forefoot pain, with non-neoplastic soft tissue lesions representing the overwhelming majority.[2-4]

Due to this wide range in forefoot disorders, MRI has become increasingly important in determining the underlying etiology. While radiologists should be somewhat familiar with the expansive list of potential causes, this case report will predominantly discuss intermetatarsal lesions.

Stress fracture

Metatarsal stress fractures are a common cause of forefoot pain.[1] Radiologists and clinicians alike should have a high index of suspicion for this condition, especially if the patient is prone to chronic repetitive forefoot stress (eg, runners, military members, gymnasts, ballet dancers, etc.). Other structural abnormalities such as hallux valgus deformity or a flattened longitudinal arch may contribute to the development of this disorder.[1,2] Stress fractures are often overlooked due to their chronic insidious manifestation. Failure to recognize and promptly treat stress fractures can lead to increased morbidity and significant time lost from the activity.

On MRI, initial stress response may appear as nonspecific amorphous marrow edema. Subsequent development of a stress fracture presents as a linear band of hypointense signal on both T1- and T2-weighted images. Other secondary findings such as cortical thickening, increased T2-signal, and enhancement of the surrounding soft tissues may also be seen. In terms of location, the middle to distal portions of the second through fourth metatarsals and the hallux sesamoids are the most commonly involved.[1,2]

Morton Neuroma

Morton neuroma is a non-neoplastic fibrosis involving the intermetatarsal nerve. The specific pathogenesis of this entity is not completely understood; however, it is likely related to nerve entrapment and subsequent neural thickening.[2-4] Prolonged forefoot weight bearing, as seen with wearing high-heeled shoes, is thought to contribute to and exacerbate this condition. For this reason, it is most common in middle-aged women.

On MRI, Morton neuroma frequently presents as a circumscribed fusiform mass that demonstrates low to intermediate signal on T1- and T2-weighted images due to its fibrous nature. Some lesions may demonstrate increased signal on T2-weighted images, presumably related to acute edematous changes.[2-4] Variable enhancement may be seen. Regarding location, Morton neuromas commonly arise between the metatarsal heads of the second and third metatarsals and extend above and below the deep transverse metatarsal ligament (DTML).[2,5] The DTML is a forefoot stabilizer composed of 4 intermetatarsal bands extending between the adjacent metatarsal heads, connecting the respective plantar plates.[5]

Intermetatarsal Bursitis

Intermetatarsal bursitis is a common cause of forefoot pain that can be related to multiple pathologies (including Morton neuroma and stress fracture), but is most frequently affiliated with degenerative joint disease.[2-4] The intermetatarsal bursae lie just above the DTML and between the interosseous tendons. The bursae of the second and third intermetatarsal spaces extend distal to the DTML and demonstrate close approximation with the respective neurovascular bundles.[5] This anatomical arrangement may contribute to the concomitant presentation of bursitis with Morton neuromas in these locations.

On MRI, intermetatarsal bursitis presents as a circumscribed fluid collection > 3 mm in diameter, which demonstrates homogeneously increased signal on T2-weighted images and decreased signal on T1-weighted images. Small intermetatarsal fluid collections, < 3 mm in diameter, are considered physiologic.[2,3,5] Intermetatarsal bursitis does not extend below the deep transverse metatarsal ligament, a key distinguishing factor from a Morton neuroma. Peripheral enhancement may be seen.

Ganglion Cyst

Ganglion and synovial cysts are terms often used interchangeably to describe cystic lesions arising from the tendon sheath and synovium.[2,3,6] They

are the most common benign soft-tissue lesions of the foot and are typically dorsal to the metatarsophalangeal joints. Ganglia are thought to be caused by repetitive trauma, as seen with degenerative joint disease, which leads to mucoid cystic neural degeneration.[6]

On MRI, ganglion cysts present as circumscribed homogeneously T2-hyperintense fluid-signal masses that demonstrate variable signal on T1-weighted images, based on proteinaceous content. An associated thin stalk may be visualized extending to the joint space. Thin peripheral and septal enhancement is common without central enhancement.[6]

Abscess (Osteomyelitis)

Abscesses and osteomyelitis in the foot are most commonly caused by transcutaneous spread of infection and may be located anywhere along the length of a sinus tract.[2] Clinical presentation is typically a diabetic patient with cellulitis and ulcers. Ulcers of the forefoot usually present along areas of high pressure, such as the plantar surfaces of the first and fifth metatarsal heads.[2]

On MRI, abscesses demonstrate increased signal on T2-weighted imaging and corresponding decreased signal on T1-weighted imaging with thick peripheral enhancement.[2] Findings of osteomyelitis are typically visualized along the adjacent osseous structures. These include decreased marrow signal on T1-weighted images, corresponding increased signal on T2-weighted images, and heterogeneous contrast enhancement. Reactive adjacent soft-tissue edema and cortical erosions may also be visualized.

Schwannoma

A schwannoma is a benign tumor that develops from Schwann cells along the peripheral nerve sheath. Combined with neurofibromas they constitute approximately 10% of all benign soft-tissue lesions.[2,7] Extremity schwannomas typically present along the flexor aspects, commonly involving the ulnar and peroneal nerves of the arm and leg. Development of a schwannoma in the foot is uncommon, with the incidence estimated as low as 1%.[7]

On MRI, schwannomas present as fusiform encapsulated lesions demonstrating increased signal on T2-weighted imaging that are eccentric to the associated nerve. Additional imaging characteristics can include a surrounding rim of fat, visualization of entering and exiting nerve roots, and a central area of decreased signal on T2-weighted images representing fibrocartilaginous tissue ("target sign").[2]

Diagnosis

Intermetatarsal bursitis

Summary

Intermetatarsal disease is one of the many pathologies that can lead to chronic forefoot pain. If an intermetatarsal lesion is identified on MRI, the location and signal characteristics can be used to suggest a specific disease process. Precise imaging diagnosis, in conjunction with the clinical history, can lead to appropriate treatment and ultimately improve patient outcome.

References

1. Cothran VE, Young CC, White RD, et al. Metatarsal stress fracture. Medscape https://emedicine.medscape.com/article/85746. Updated November 2016. Accessed November 5, 2017.
2. Ashman CJ, Klecker RJ, Yu JS. Forefoot pain involving the metatarsal region: differential diagnosis with MR imaging. Radiographics 2001;21(6):1425-1440.
3. Van Hul E, Vanhoenacker F, Van Dyck P, et al. Pseudotumoural soft tissue lesions of the foot and ankle: a pictorial review. Insights Imaging 2011;2(4):439-452.
4. Bermejo A, De Bustamante TD, Martinez A, et al. MR imaging in the evaluation of cystic-appearing soft-tissue masses of the extremities. Radiographics 2013;33(3):833-855.
5. Theumann NH, Pfirrmann CW, Chung CB, et al. Intermetatarsal spaces: analysis with MR bursography, anatomic correlation, and histopathology in cadavers. Radiology 2001;221(2):478-484.
6. Neto N, Nunnes P. Spectrum of MRI features of ganglion and synovial cysts. Insights Imaging 2016;7(2):179-186.
7. Albert P, Patel J, Badawy K, et al. Peripheral nerve schwannoma: a review of varying clinical presentations and imaging findings. J Foot Ankle Surg 2017;56(3):632-637.

Large Fatty Soft-tissue Mass

Brandon Mason, D.O., Jonathon Kirkland, D.O., Donald von Borstel, D.O.

Department of Radiology, Oklahoma State University Medical Center, Tulsa, OK

Case Presentation

A 49-year-old woman presented with a 1-year history of a painless mass growing in her right posterior thigh. On physical examination, a palpable soft-tissue mass, which increased on follow-up visits, was noted in the posterior thigh. The patient had progressive discomfort without neurovascular symptoms. Over the course of the year, she had an ultrasound of the mass, and it was diagnosed as a likely benign lipoma. She was subsequently referred for MRI of the thigh with and without contrast to further characterize the mass.

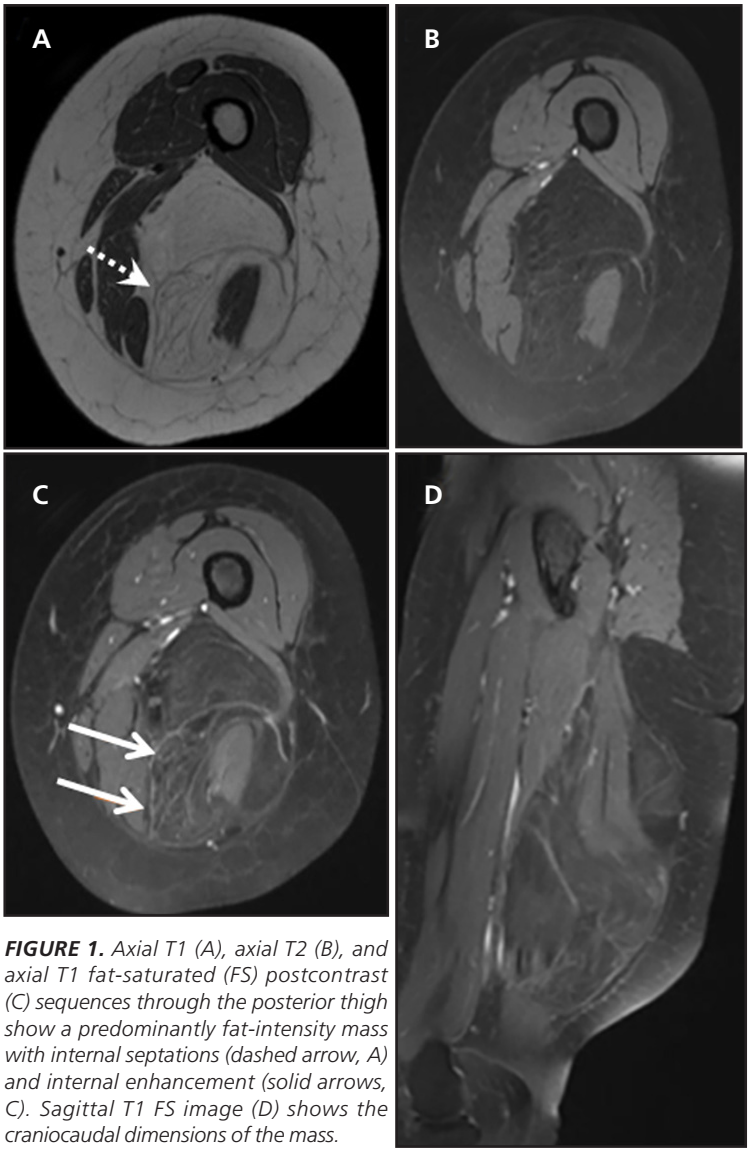

FIGURE 1. *Axial T1 (A), axial T2 (B), and axial T1 fat-saturated (FS) postcontrast (C) sequences through the posterior thigh show a predominantly fat-intensity mass with internal septations (dashed arrow, A) and internal enhancement (solid arrows, C). Sagittal T1 FS image (D) shows the craniocaudal dimensions of the mass.*

Key Imaging Finding

Fat signal intensity soft-tissue mass with internal septations and enhancement

Differential Diagnosis

Well-differentiated liposarcoma (atypical lipomatous neoplasm)
Lipoma
Spindle cell lipoma

Discussion

A soft-tissue mass in the appendicular skeleton can be a concerning clinical finding, although most soft-tissue lesions in extremities are benign. Ultrasound can be used as a first-line imaging tool to determine the anatomical location of the mass and the primary type of tissue involved. MRI is the gold standard imaging tool to determine the tissue composition, as well as additional important imaging characteristics, including enhancement pattern and involvement of adjacent soft tissues and compartments. If the soft-tissue mass has concerning clinical characteristics or a malignant appearance on imaging, biopsy or resection is indicated for definitive diagnosis.

Well-differentiated liposarcoma

Well-differentiated liposarcoma (atypical lipomatous neoplasm) is most common in the extremities and retroperitoneum. They have a slight male predominance and usually occur in the fifth decade of life. Patients typically describe a slow-growing soft-tissue mass that only becomes painful or symptomatic when the tumor becomes very large. On gross pathologic examination, the specimen is typically well-circumscribed, soft, and lobulated. Areas of fat necrosis may be seen in large lesions. Histologic characteristics show mature adipocytic cells, atypical stromal cells, and scattered lipoblasts.[1] The lesion demonstrates a positive *MDM2* amplification by fluorescence in-situ hybridization (FISH)[2] and overexpression of *HMGA2* and the cyclin-dependent kinase *CDK4*.

On radiography, internal calcifications may or may not be seen within the lesion. If the lesion is aggressive/high-grade, associated osseous erosions may be present. Ultrasound typically demonstrates a well-circumscribed and lobulated hyperechoic mass that is often difficult to distinguish from a lipoma. CT demonstrates a lobulated fat-attenuating mass with well-defined margins. The presence of internal septations and enhancement are variable. Osseous erosions can be seen in higher-grade lesions. MRI demonstrates a well-defined and lobulated mass with an identifiable capsule. These masses are T1- and T2-hyperintense due to fat content with variable internal hypointense septations. Signal dropout is seen on fat-suppressed sequences. Variable internal septal enhancement is seen on T1-weighted, fat-suppressed postcontrast images. Treatment typically requires wide-margin resection of the mass with favorable outcomes. Postresection radiation therapy of the surgical bed has been utilized in some cases.

Lipoma

A lipoma is a benign soft-tissue mass that makes up nearly 50% of all soft-tissue masses. On histology, they typically cannot be differentiated from normal adipose tissue.[3] Lipomas are encapsulated, and the attenuation of the capsule is similar to muscle. Lipomas are typically smaller than a well-differentiated liposarcoma and are typically < 10 cm. A lipoma will commonly show homogeneous fat attenuation on CT and fat signal intensity on all MRI pulse sequences. Small septations, < 2 mm thick, may be noted within the lipoma and they may or may not display a peripheral capsule on imaging.[3] Lipomas lack the typical thickened septations and internal enhancement that can be seen in more aggressive entities.

Spindle Cell Lipoma

Spindle cell lipomas are a benign form of lipoma that are typically seen in the superficial soft tissues. Spindle cell lipomas have a male predominance and are typically diagnosed between 45 to 65 years of age. These lesions predominantly occur in the posterior neck, shoulder, and back.[4] Spindle cell lipomas typically demonstrate increased heterogeneity on imaging (CT and MRI) in relation to lipomas and well-differentiated liposarcoma. This is due to internal areas of nonadipose tissue, which are typically present at a greater ratio compared to an atypical lipomatous neoplasm. Spindle cell lipomas commonly demonstrate avid enhancement of the nonadipose tissue on postcontrast CT and MRI.

Diagnosis

Well-differentiated liposarcoma (atypical lipomatous neoplasm)

Summary

MRI is important in the imaging workup and management of patients with a soft-tissue mass in the appendicular skeleton. The primary role of MRI is to determine tissue composition of the mass, enhancement characteristics, and relation of the mass to adjacent neurovascular and musculoskeletal structures. The differential diagnosis for a fatty soft-tissue mass in the appendicular skeleton includes a well-differentiated liposarcoma, lipoma, and spindle cell lipoma. The MRI characteristics of these lesions help determine the appropriate follow-up and whether surgical resection is warranted.

References

1. Brisson M, Kashima T, Delaney D, et al. MRI characteristics of lipoma and atypical lipomatous tumor/well-differentiated liposarcoma: retrospective comparison with histology and MDM2 gene amplification. Skeletal Radiol 2013;42(5):635-647.
2. Clay MR, Martinez AP, Weiss SW, et al. MDM2 amplification in problematic lipomatous tumors: analysis of FISH testing criteria. Am J Surg Pathol 2015;39(10):1433-1439.
3. Kransdorf MJ, Bancroft LW, Peterson JJ, et al. Imaging of fatty tumors: distinction of lipoma and well-differentiated liposarcoma. Radiology 2002;224(1):99-104.
4. Bancroft LW, Kransdorf MJ, Peterson JJ, et al. Imaging characteristics of spindle cell lipoma. Am J Roentgenol 2003;181(5):1251-1254.

JAOCR at the Viewbox

Leomar Bautista D.O., Peter Mostert D.O.

Department of Radiology, Oklahoma State University Medical Center, Tulsa, OK

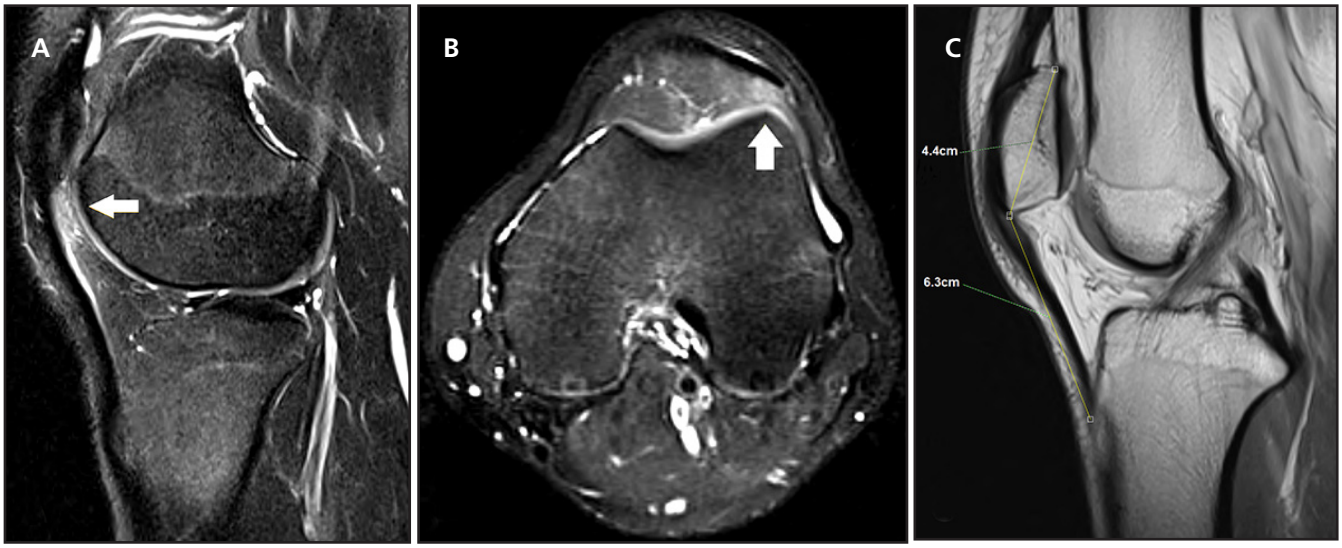

Patellar Tendon-Lateral Femoral Condyle Friction Syndrome

A 34-year-old man with chronic anterior knee pain underwent MRI after a radiograph of the left knee demonstrated no acute or significant degenerative findings. Sagittal and axial short TI inversion recovery (STIR) images (**A and B, respectively**) demonstrated increased signal at the superolateral aspect of the infrapatellar fat pad (solid arrows), and the Insall-Salvati ratio (**C, dashed line/solid line**) was 1.4.

Patellar tendon-lateral femoral condyle friction syndrome (Hoffa fat pad impingement) is thought to be an overuse injury characterized by direct contact of the patellar tendon against the lateral femoral condyle, causing compression of the superolateral aspect of the infrapatellar fat pad.[1,2] The etiology of this syndrome is likely due to altered biomechanics and may be associated with patellar maltracking and a weakened vastus medialis muscle. This syndrome typically affects younger adults but can affect those aged 13 to 56 years. It is more common in individuals who do not participate in routine athletic activities.[2]

The diagnosis is classically made with MRI and usually occult on radiography and CT. MRI findings include increased focal T2-signal at the superolateral aspect of the infrapatellar fat pad. Other associated findings include lateral patellar subluxation/maltracking and increased Insall-Salvati ratio of > 1.2 (patella alta). Conservative treatment is usually successful, although full recovery may take time. Over the counter anti-inflammatory medications and taping/bandaging of the superior pole of the patella to relieve pressure of the infrapatellar fat pad have proven to result in high treatment success rates.[1]

References

1. Chung CB, Skaf A, Roger B, et al. Patellar tendon-lateral femoral condyle friction syndrome: MR imaging in 42 patients. Skeletal Radiol 2001;30(12):694-697.
2. Bergman AG, Fredericson M. MR imaging of stress reactions, muscle injuries, and other overuse injuries in runners. Magn Reson Imaging Clin N Am 1999;7(1):151-174.

JAOCR at the Viewbox

Heather Ivy, D.O., Damon Brooks, D.O.

Department of Radiology, Oklahoma State University Medical Center, Tulsa, OK

Erosive Osteoarthritis

A 74-year-old woman presented to her primary care physician complaining of worsening hand pain and stiffness. She had tried various nonsteroidal anti-inflammatory drugs, but her pain increased over time. The physician noticed hypertrophy, erythema, and tenderness of the interphalangeal joints on physical examination and ordered hand radiographs for further characterization. Frontal radiographs (**A**) revealed symmetric proximal and distal interphalangeal joint space narrowing, subchondral sclerosis, marginal osteophytes, and erosions. The erosions demonstrated the characteristic "gull-wing" appearance (**B**) of erosive osteoarthritis. She also had degenerative changes of the first carpometacarpal joints (**A**).

Erosive osteoarthritis (EOA) is the inflammatory version of osteoarthritis found predominantly in postmenopausal women. The erosions mimic changes found in rheumatoid arthritis (RA); however, patients' clinical findings and radiologic distribution of erosions differ from RA. The typical distribution of EOA involves the proximal and distal interphalangeal joints and first carpometacarpal joints of the hands, similar to osteoarthritis. Although less likely, EOA may also involve the hip, knee or facets of the cervical spine.[1] RA characteristically involves the metacarpophalangeal joints as well as the carpometacarpal, intercarpal, and radiocarpal joints of the wrist.[1]

Abrupt onset of pain, swelling, redness, warmth, and limited hand function are common in most patients with EOA. EOA is usually a self-limiting disease with residual deformity after the acute arthritic stage has passed; however, some cases occasionally progress to long-term clinical manifestations such as RA.[2]

References

1. Keats TE, Johnstone WH, O'Brien WM. Large joint destruction erosive osteoarthritis. Skeletal Radiol 1981;6(4):267-269.
2. Chew FS. Radiology of the hands: review and self-assessment module. Am J Roentgenol 2005;184:S157-168.

JAOCR at the Viewbox

Corey R. Matthews, D.O., Jeremy S. Fullingim, D.O.

Department of Radiology, Oklahoma State University Medical Center, Tulsa, OK

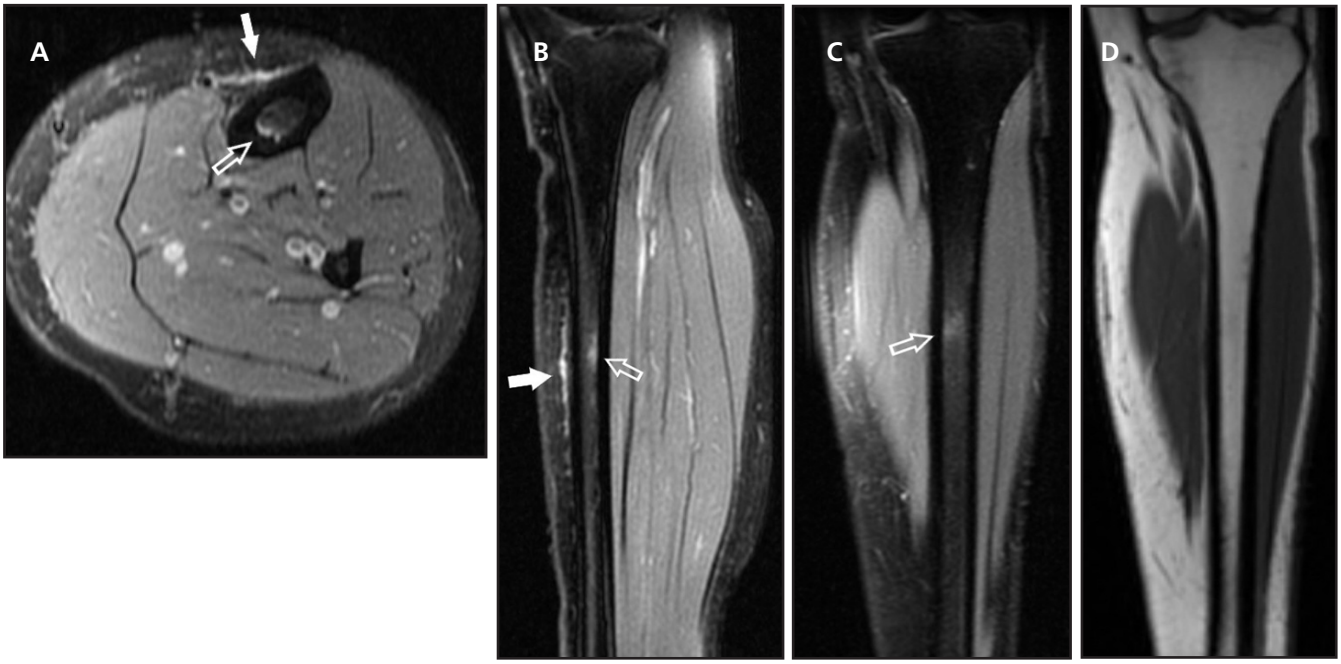

Medial Tibial Stress Syndrome

A 38-year-old runner presented to her primary care physician with chronic left shin pain that was aggravated by running. After normal radiographs, an MRI was obtained. Fat-suppressed proton density images (**A-C**) demonstrated hyperintense pretibial periosteal edema-like signal (**solid arrow, A and B**) with mild focal increased marrow signal in the adjacent tibial diaphysis (**open arrow, A-C**). Marrow signal on T1-weighted imaging (**D**) was normal with no discrete fracture seen. These findings highly suggested grade II medial tibial stress syndrome (MTSS).

MTSS is a painful condition that is most commonly self-limiting and usually improves with conservative therapy. It tends to affect athletes, especially runners, and likely represents a stress reaction from repetitive microtrauma. MTSS is more common in females and is often recurrent.

MRI findings and their associated classification (Fredericson) are as follows: periosteal edema only (grade I), periosteal edema with increased marrow signal on T2 (grade II), periosteal edema with increased T2 signal and decreased T1signal (grade III), and multiple nonlinear (grade IVa) or linear (grade IVb) cortical signal changes. These grades positively correlate with the time required for complete healing, with grade I taking 2 to 3 weeks, grades II-IVa taking 6 to 7 weeks, and grade IVb taking 9 to 10 weeks or more.[1,2] Contrarily, pain level with activity negatively correlates with both time to complete healing and MRI grade severity.[1] Therefore, MRI has better prognostic utility for athletes with suspected MTSS than clinical history alone. Additionally, MRI can help rule out acute fractures, muscle injury, and other less common causes of shin pain.

References

1. Beck BR, Bergman AG, Miner M, et al. Tibial stress injury: relationship of radiographic, nuclear medicine bone scanning, MR imaging, and CT severity grades to clinical severity and time to healing. Radiology 2012;263(3):811-818.
2. Kijowski R, Choi J, Shinki K, et al. Validation of MRI classification system for tibial stress injuries. Am J Roentgenol 2012;198(4):878-884.